AEDC-TR-88-37

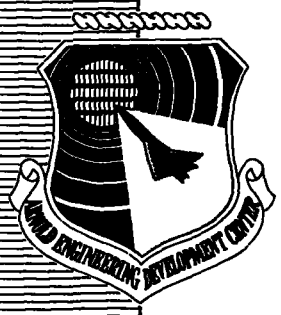

Supersonic Particle Probes: Measurement of Internal Wall Losses

J. J. Ivie, L. J. Forney, and R. L. Roach
Georgia Institute of Technology
Atlanta, Georgia 30332-0100

March 1989

Final Report for Period June 10, 1986 – June 10, 1988

ARNOLD ENGINEERING DEVELOPMENT CENTER
ARNOLD AIR FORCE BASE, TENNESSEE
AIR FORCE SYSTEMS COMMAND
UNITED STATES AIR FORCE

NOTICES

When U. S. Government drawings, specifications, or other data are used for any purpose other than a definitely related Government procurement operation, the Government thereby incurs no responsibility nor any obligation whatsoever, and the fact that the Government may have formulated, furnished, or in any way supplied the said drawings, specifications, or other data, is not to be regarded by implication or otherwise, or in any manner licensing the holder or any other person or corporation, or conveying any rights or permission to manufacture, use, or sell any patented invention that may in any way be related thereto.

Qualified users may obtain copies of this report from the Defense Technical Information Center.

References to named commercial products in this report are not to be considered in any sense as an endorsement of the product by the United States Air Force or the Government.

This report has been reviewed by the Office of Public Affairs (PA) and is releasable to the National Technical Information Service (NTIS). At NTIS, it will be available to the general public, including foreign nations.

APPROVAL STATEMENT

This report has been reviewed and approved.

Marjorie S. Collier

MARJORIE S. COLLIER
Directorate of Technology
Deputy for Operations

Approved for publication:

FOR THE COMMANDER

Keith L Kushman

KEITH L. KUSHMAN
Technical Director
Directorate of Technology
Deputy for Operations

UNCLASSIFIED
SECURITY CLASSIFICATION OF THIS PAGE

REPORT DOCUMENTATION PAGE

Form Approved OMB No. 0704-0188

1a REPORT SECURITY CLASSIFICATION: UNCLASSIFIED	1b RESTRICTIVE MARKINGS
2a. SECURITY CLASSIFICATION AUTHORITY	3 DISTRIBUTION/AVAILABILITY OF REPORT: Approved for public release; distribution is unlimited.
2b. DECLASSIFICATION/DOWNGRADING SCHEDULE	
4. PERFORMING ORGANIZATION REPORT NUMBER(S): AEDC-TR-88-37	5. MONITORING ORGANIZATION REPORT NUMBER(S)
6a. NAME OF PERFORMING ORGANIZATION: Georgia Tech Research Corporation; 6b. OFFICE SYMBOL (If applicable)	7a. NAME OF MONITORING ORGANIZATION
6c. ADDRESS (City, State, and ZIP Code): Centennial Research Building, Room 246, Georgia Institute of Technology, Atlanta, GA 30332-0420	7b. ADDRESS (City, State, and ZIP Code)
8a. NAME OF FUNDING/SPONSORING ORGANIZATION: Arnold Engineering Development Center; 8b. OFFICE SYMBOL (If applicable): DO	9 PROCUREMENT INSTRUMENT IDENTIFICATION NUMBER: F40600-86-K004
8c. ADDRESS (City, State, and ZIP Code): Air Force Systems Command, Arnold Air Force Base, TN 37389-5000	10. SOURCE OF FUNDING NUMBERS: PROGRAM ELEMENT NO. 65807F; PROJECT NO.; TASK NO; WORK UNIT ACCESSION NO

11. TITLE (Include Security Classification)

Supersonic Particle Probes: Measurement of Internal Wall Losses

12. PERSONAL AUTHOR(S)

Ivie, J. J., Forney, L. J., and Roach, R. L., Georgia Institute of Technology

13a. TYPE OF REPORT	13b TIME COVERED	14. DATE OF REPORT (Year, Month, Day)	15. PAGE COUNT
Final	FROM 6/10/86 TO 6/10/88	March 1989	106

16. SUPPLEMENTARY NOTATION

Available in Defense Technical Information Center (DTIC).

17. COSATI CODES			18. SUBJECT TERMS (Continue on reverse if necessary and identify by block number)
FIELD	GROUP	SUB-GROUP	particle sampling; wall losses; supersonic; particle probe
20	07		
14	02		

19. ABSTRACT (Continue on reverse if necessary and identify by block number)

In the present study, the operating characteristics of supersonic particle probes were investigated. The characteristics such as internal wall deposition, pressure recovery, and ease of operation and construction were examined. Three basic probe designs were tested in a cold flow experiment designed to simulate the hot, hostile environment of rocket and jet engine plumes. The probe designs consisted of two internal shock probes (Dehne and Colket probes) and one external shock probe (McGregor probe). In the internal shock probes, the compression from supersonic to subsonic flow occurred either in a constant area throat (Dehne) or at a sudden expansion (Colket). In the external shock, or McGregor probe, the shock was positioned slightly outside the entrance of the probe. From deposition studies performed on the probes, three factors were found to enhance deposition. These factors were (1) shock-boundary layer interaction, (2) particle-boundary layer interaction, and (3) stagnation zones at sudden expansions. The probe with the lowest deposition was a McGregor probe with a 2.0-deg divergence angle. Using test (Cont)

20. DISTRIBUTION/AVAILABILITY OF ABSTRACT	21. ABSTRACT SECURITY CLASSIFICATION	
☐ UNCLASSIFIED/UNLIMITED ☒ SAME AS RPT. ☐ DTIC USERS	UNCLASSIFIED	
22a NAME OF RESPONSIBLE INDIVIDUAL: C. L. Garner	22b TELEPHONE (Include Area Code): (615) 454-7813	22c. OFFICE SYMBOL: DOCS

DD Form 1473, JUN 86 — Previous editions are obsolete. — SECURITY CLASSIFICATION OF THIS PAGE

UNCLASSIFIED

19. ABSTRACT (Concluded)

particles with diameters of 1.0, 1.5, 2.0, and 2.5 μm, the average losses in the McGregor probe were 14 percent, whereas in the Colket and Dehne probes, the losses were 18 and 22 percent, respectively. A correlation was developed to predict the deposition (E) in the McGregor probe using Willeke's dimensionless parameter (Ω): $E = 1011\ \Omega + 1.55$. Pressure recovery was also found to be the greatest in the McGregor probe with 48 percent of the initial stagnation pressure regained. The Colket probe had only a 7-percent pressure recovery. On the other hand, the McGregor probe was found to be the most difficult to operate. In this probe the back pressure had to be controlled to within a few percent of a set value so that the shock would be positioned slightly outside of the probe entrance. In terms of manufacturing difficulty, the Colket probe presented the most problems because of the need for smooth internal surfaces to prevent premature shocks within the supersonic throat of the probe.

PREFACE

The work reported herein was sponsored by the Air Force Systems Command (AFSC) under contract F40600-86-K0004 for the Arnold Engineering Development Center (AEDC), AFSC, Arnold Air Force Station, Tennessee. The contract officers were Captain Bradley Bien and Ms. Marjorie Collier for the Directorate of Technology (DOT), AFSC. Assistance was also provided by Robert Reed and William McGregor of Sverdrup Technology, Inc., the operating contractor for propulsion testing at the AEDC, AFSC.

TABLE OF CONTENTS

LIST OF ILLUSTRATIONS

LIST OF TABLES

1.0 INTRODUCTION

During the operation of rocket and jet engines, particles are formed from the condensation of super-saturated vapor formed in the combustion process. The small submicron particles coagulate and grow into larger liquid and solid particles. In the evaluation of the performance of rocket and jet engines, an idea of the size, concentration, and composition of the particles is needed. For example, the size and concentration of the alumina oxide droplets formed in solid propellant rocket engines influences the thrust characteristics of the engine. Also, the physical characteristics of the alumina oxide droplets or the organic agglomerates found in jet engines affect the radiative heat transfer rates to the internal surfaces of the engines.

In recent years non-intrusive measurement techniques (optical methods) have gained popularity in measuring particle sizes and concentrations. Though these methods have many inherit advantages, they do have drawbacks. Flows with an excessively high concentration of particles usually cannot be evaluated with non-intrusive methods. Also, situations in which the particles possess a high luminescence can limit the applicability of the non-intrusive techniques. In addition to these drawbacks, the non-intrusive methods must be calibrated which requires the use of particle probes to provide a direct sampling of the particles.

With the need for particle sampling probes established, good probe characteristics must be determined. The probes must be able to withstand the high temperature and abrasive environment found in rocket and jet engine plumes. The probes must provide a representative sample of particles in these

flows without being prejudicial toward or against a particular size class of particles. Moreover, the probe should have low particle deposition rates on the internal walls of the probes with good pressure recovery characteristics. With these factors in mind, the evaluation of different probe designs may proceed.

Although considerable time has been spent on the development of various probe designs [1,2,3,4,5], little fundamental work has been done experimentally or theoretically to determine the magnitude of the particle deposition on the walls of the different probes or the size bias caused by the probes. In the present report, a method of evaluating different probe designs is presented. In the evaluation procedure, the hot flows found in the rocket and jet engines were modeled with a cold flow experiment. Consequently, the procedure presented concentrates on the particle sampling and wall deposition characteristics of the probes while ignoring the significant material problem associated with the hostile environment in which the probes are subjected.

Initially, three probe designs were proposed to be evaluated. Because the particles sampled by the probes were found in supersonic gas flows, the positioning of the shock induced by the probe was considered an important factor in the performance of the probe. One of the probe designs evaluated positioned the shock just outside the probe entrance (external shock probe) while the other two probe designs swallowed the shock (internal shock probes).

The purpose of the present work was to measure and compare the internal wall losses in the three fundamental probe designs. With the effect of particle deposition quantified for the different probes, a recommendation on the best probe design was made. Also, other probe properties such as pressure recovery characteristics and ease of construction have been compared.

2.0 SUPERSONIC PROBE DESIGN

The main functions of the supersonic particle probes are to collect a representative sample of particles from a supersonic flow, slow the collected particles to subsonic speeds, and ultimately bring the particles to rest so that they may be characterized. In supersonic probes the way in which the deceleration process occurs leads to three possibilities:

1. External shock probes
2. Internal shock probes
3. Isentropic (shockless) probes.

The sampling or capture efficiency of the various probes is determined by the flow field conditions found at the entrance of the probes. The shockless or internal shock probes have capture efficiencies close to 100 % because flow field disturbances are minimized. The sharp leading edges of these probes cause only small deviations in the streamlines of the flow field, therefore, causing only small deviations in the trajectories of the particles. Because all gas exposed to probe entrance is ingested by the probe, most if not all of the particles exposed to the entrance are ingested. On the other hand, the high back pressure of the external shock probe may lead to pronounced deviations in the streamlines of the flow field and trajectories of the particles. Collection efficiencies for the external shock probe are usually less than the shockless or internal shock probes [6].

Although better collection efficiencies are an advantage of the shockless and internal shock probes, drawbacks in these probes are present. The design of a shockless probe entrance is difficult and the probe is limited in application to the design Mach number. The sharp leading edges on the shockless and internal shock probes are susceptible to the erosive environment found in the exhaust plumes. Furthermore, pressure monitoring within the internal shock probes is required to ensure that the shock is swallowed. Also, to stabilize the position of the shock within the probe and to reduce velocities to low Mach numbers (<0.1) so that no choking occurs in the sample lines; sudden expansions, sharp turning angles, or rough probe surfaces may be necessary. All of these factors enhance unwanted flow separation and recirculation that lead to particle impaction on the internal surfaces of the probe. With these factors in mind, three existing probe designs are proposed to be evaluated. The characteristics of each design are discussed in the following sections.

2.1 DEHNE PROBE DESIGN (Internal Shock)

The Dehne probe design which is pictured in Fig. 2.1 was developed by H.J. Dehne of the Acurex Corporation [4]. As shown in Fig. 2.1 the probe features a sharp leading edge at the probe entrance. The first section encountered by the particles as they enter the probe is a supersonic expansion. The particles then enter a constant area throat which contains the shock train that slows the particles to subsonic speeds. With this constant area section, the pressure recovery characteristics are enhanced. The particles then enter a subsonic diffuser that slows the particle velocity below Mach 0.1 so that no choking of the flow occurs in the sample lines.

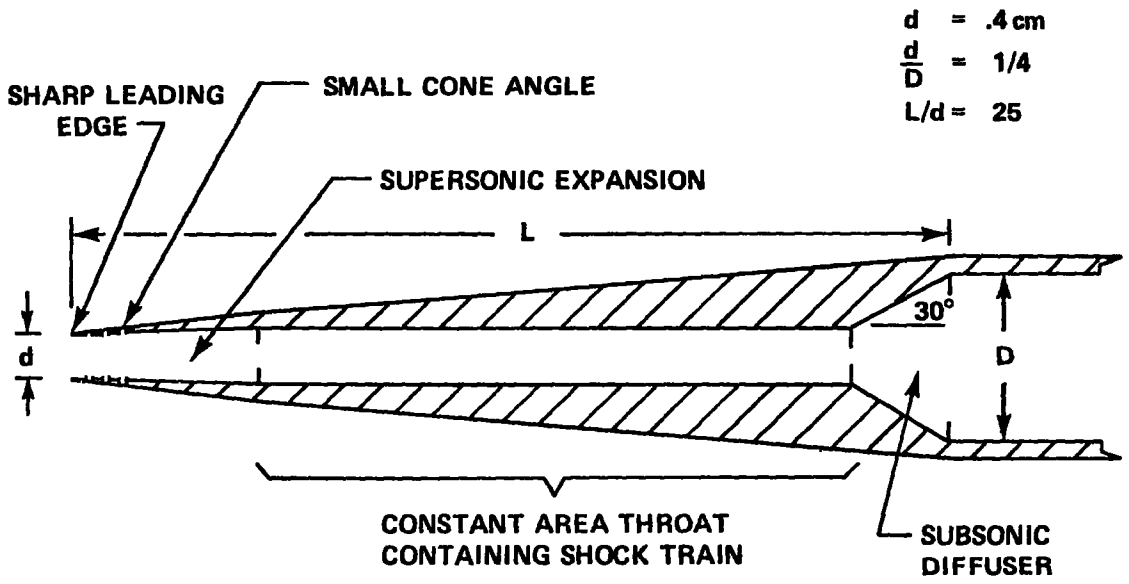

Figure 2.1. General Schematic of Dehne Probe Design (Internal Shock Probe).

After the subsonic diffuser the particles are taken by a sample line to a filter that collects the particles.

Unlike the original Dehne design [4], no boundary layer trips were included in the supersonic expansion section of the probe. The purpose of the trips was to enhance boundary layer development which would initiate and stabilize the shock train in the constant area throat. Because it is difficult to construct boundary layer trips (surface roughness), a larger cone angle was used in the supersonic expansion. The larger cone angle led to a stronger oblique shock at the corner where the expansion section met the constant area throat section. The oblique shock caused by the sharp corner triggered and stabilized the shock train within the constant area throat. In the present work two Dehne probes are studied: Dehne 1 and Dehne 2. A detailed drawing of Dehne 1 and Dehne 2 appears in Figs. 2.2 and 2.3, respectively. The only internal difference between the probes is that Dehne 1 has the 30 ° subsonic diffuser as pictured in Fig. 2.2. In Dehne 2 the subsonic diffuser is replaced with a sudden expansion. In studying the two probes the importance of the subsonic diffuser angle is investigated.

The probe geometry provides a length of five nozzle diameters for the supersonic expansion section. Following the expansion section is the constant area throat that is twenty nozzle diameters in length. The compression shock of the probe is located in the first 8 to 10 nozzle diameters of the throat section. As stated earlier, a 30° subsonic expansion is used after the throat section to reduce the velocity of the flow in Dehne 1 while in Dehne 2 a sudden expansion is used. The ratios of the nozzle diameter to sample line diameter and throat length to nozzle diameter are 1/4 and 25, respectively. These geometric ratios are maintained and used in the other probe designs presented.

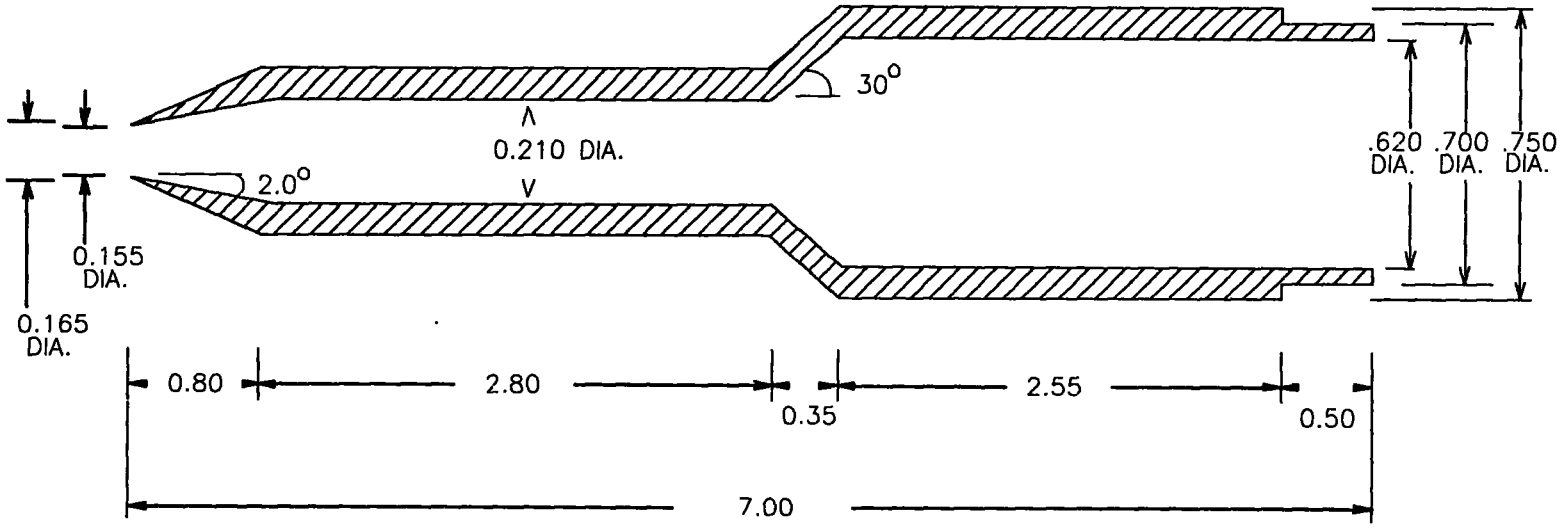

Figure 2.2. Detailed Drawing of Dehne 1 Probe. The Dimension Units are inches and the Tolerances : Length = 0.01 in., Diameter = 0.005 in.

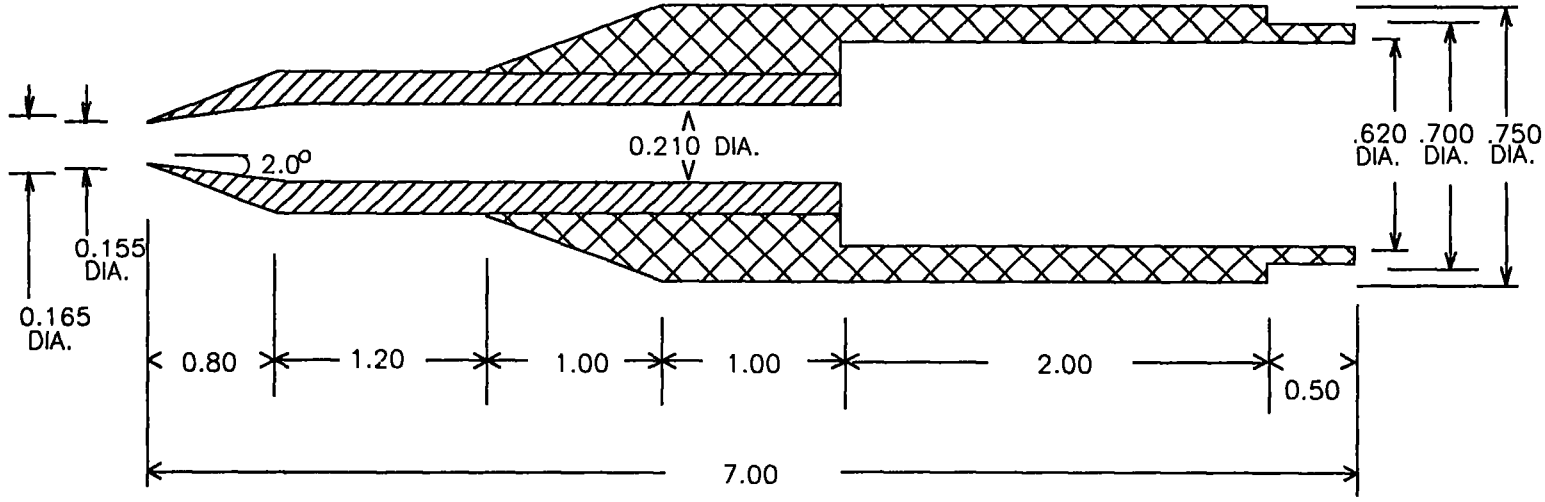

Figure 2.3. Detailed Drawing of Dehne 2 Probe. The Dimension Units are inches and the Tolerances : Length = 0.01 in., Diameter = 0.005 in.

2.2 COLKET PROBE DESIGN (Internal Shock)

The Colket probe design shown in Fig. 2.4 is similar to the design proposed by Colket et al. [7]. The original purpose of the probe was to sample hot reacting gases from flames at temperatures up to 1800 K. By accelerating the gases to supersonic speeds, the static temperature of the gas sample was reduced and quenching of the chemical reactions occurred in the sample. Next, the sample was subjected to a compression shock that caused an increase in the static temperature; but because of the convective heat transfer that occurred in the supersonic section of the probe, the static temperature was maintained below 1000 K effectively quenching the reactions.

In the original design a large area expansion is used to accelerate the sample to a high Mach number to get the desired quenching. However, in the present case the flow is already traveling at supersonic speeds so smaller area ratios can be used. Though the static temperature reduction is smaller in the present case, the temperature at the exit plane of a typical rocket nozzle is 1500 K. Since the temperature is lower than the initial 1800 K reported by Colket, smaller area ratios are used in the nozzle to enhance the pressure recovery characteristics of the nozzle.

As shown in Fig. 2.4, the Colket probe design has the sharp leading edge and supersonic expansion section similar to the Dehne probes (especially Dehne 2). Unlike the Dehne probes, the Colket probe uses the constant area section to promote the convective cooling of the sample. Also in contrast with the Dehne probes, the Colket probe design has an aerodynamically smooth transition between the supersonic expansion and the constant area throat. By eliminating the sharp corner, the compression waves do not coalesce into an oblique shock that could start a shock train in the constant

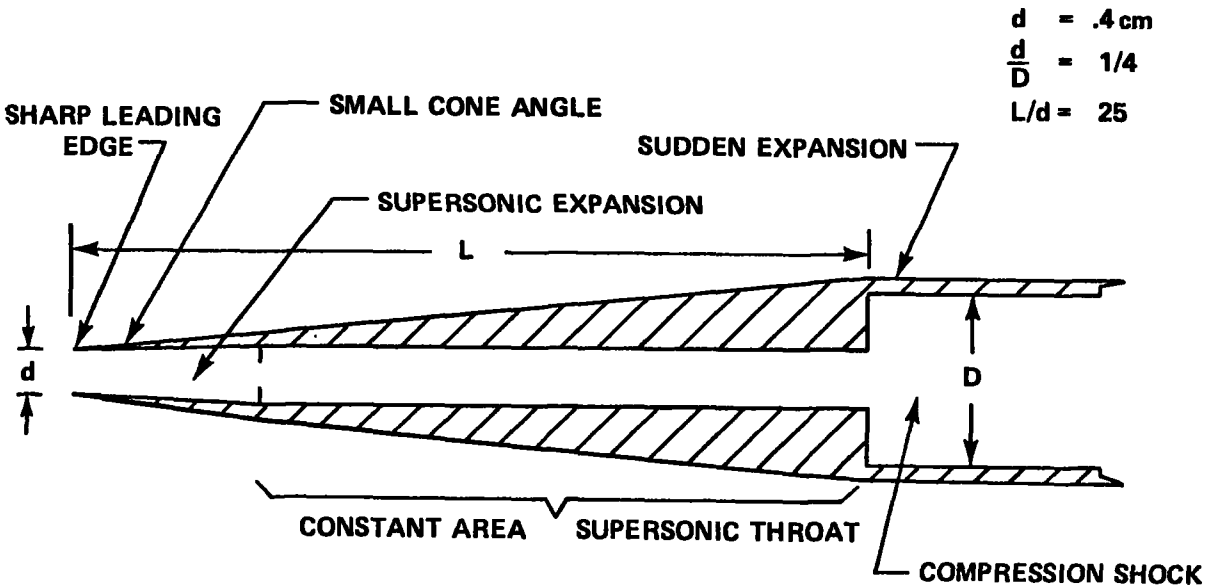

Figure 2.4. General Schematic of Colket Probe Design (Internal Shock Probe).

area throat. The shock in the Colket probe is located after the sudden expansion found at the end of the constant area section. The sudden expansion stabilizes the position of the shock within the sample tube.

In the present work two Colket probes were studied: Colket 1 and Colket 2. A detailed drawing of these probes appears in Figs. 2.5 and 2.6. In comparing the two probes, the internal structure of Colket 2 is the same as Colket 1 except that the supersonic constant area throat is removed. In the Colket 2 probe the sudden expansion which triggers the shock is positioned after the supersonic diffuser. By removing the supersonic constant area throat, the large frictional losses associated with supersonic flow may be eliminated. As a result, better pressure recovery and ease of operation may be achieved.

2.3 MCGREGOR PROBE DESIGN (external shock)

Considered the simplest of the particle probes investigated here, the McGregor probe design is illustrated in Fig. 2.7 and is taken from a design by McGregor [8]. Unlike the previous probe designs, the McGregor probe is operated with a sufficiently high back pressure so that the shock occurs outside the entrance of the probe. Consequently, the probe's basic function is similar to a subsonic diffuser that reduces the velocity of the particle-laden stream.

As shown in Fig. 2.7, the probe area expands at a cone angle from the probe entrance to probe exit. With the small cone angle ($<5^{\circ}$) and the absence of shocks, flow separation which reduces the pressure recovery of the other probes should be reduced. Also, particle deposition within the probe should be less because the aerodynamically smooth streamlines within the probe reduce separation. The main disadvantage to the external shock probe is the potential for streamline curvature behind the shock located at the probe entrance. As with

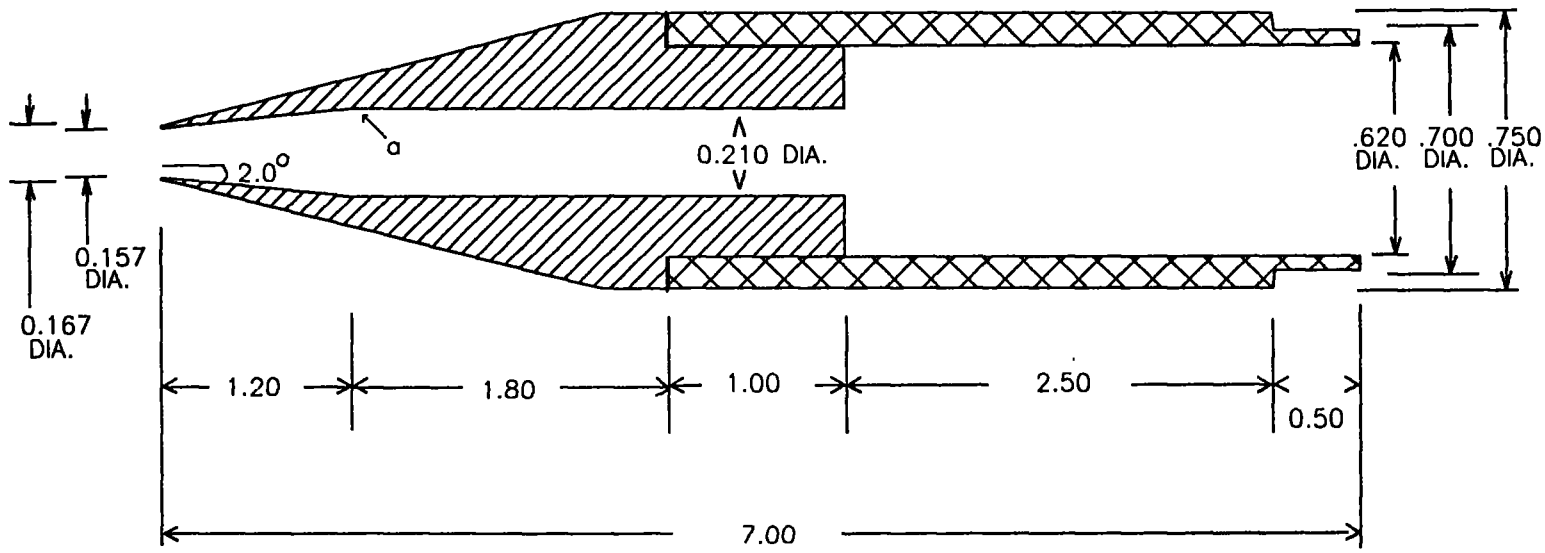

Figure 2.5. Detailed Drawing of Colket 1 Probe. The Dimension Units are inches and the Tolerances : Length = 0.01 in., Diameter = 0.005 in.

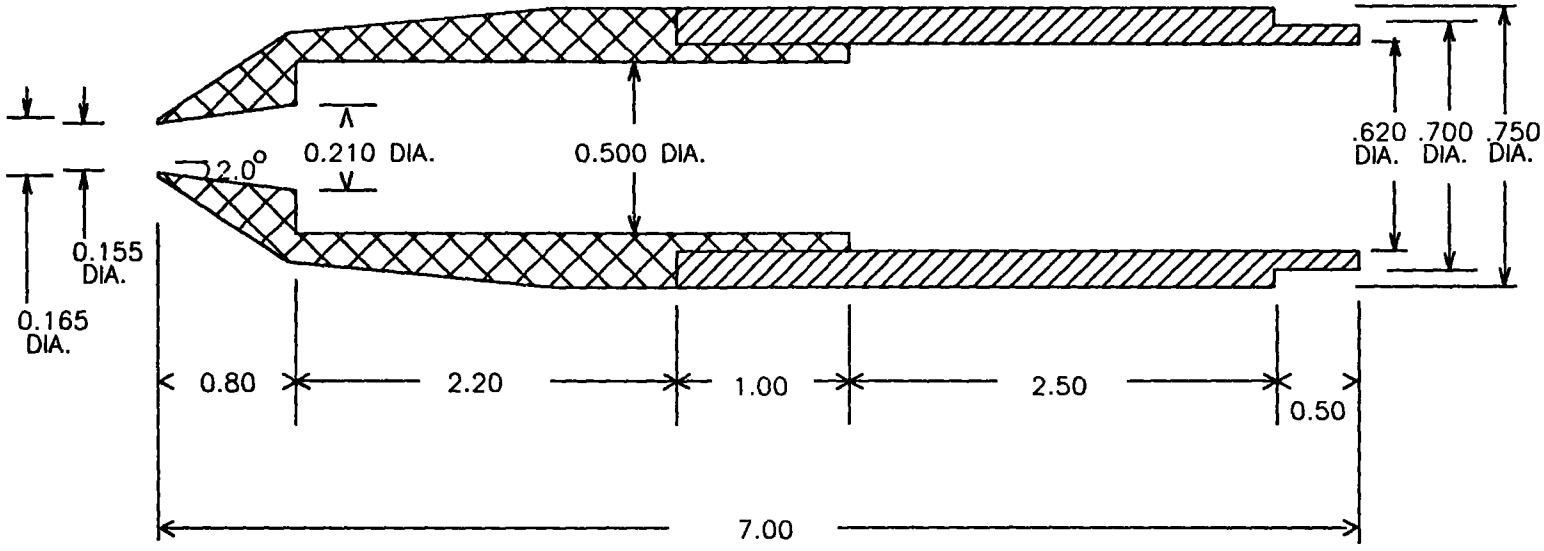

Figure 2.6. Detailed Drawing of Colket 2 Probe. The Dimension Units are inches and the Tolerances : Length = 0.01 in., Diameter = 0.005 in.

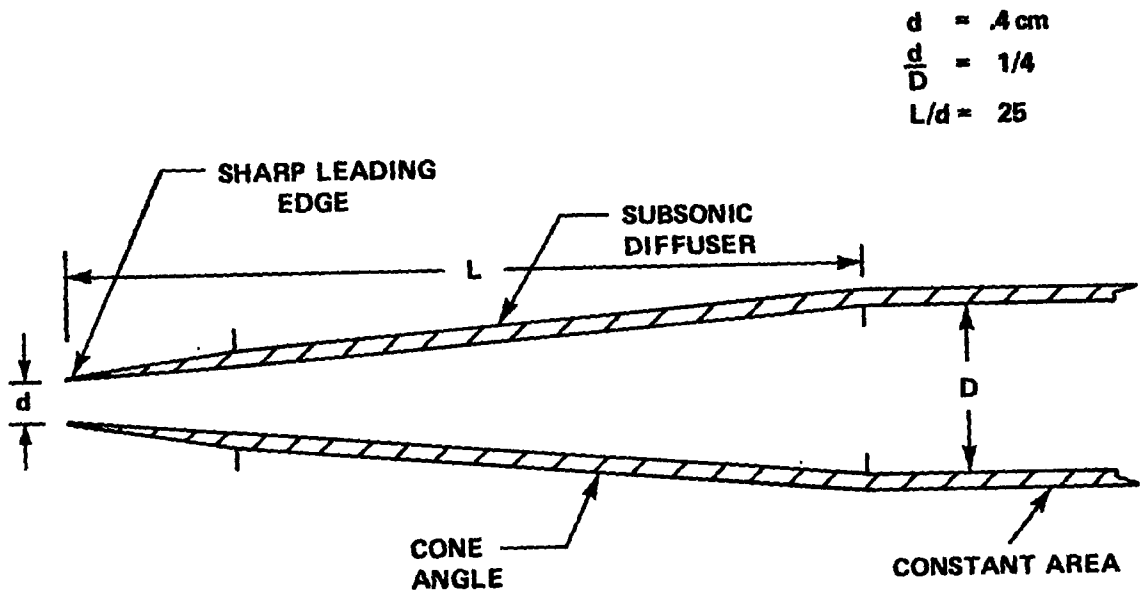

Figure 2.7. General Schematic of McGregor Probe Design (External Shock Probe).

the other probes, similar geometric ratios are used. The probe entrance to sample line diameter ratio and the throat length to entrance diameter are the same at 1/4 and 25, respectively.

In the present study, three McGregor probes were studied. Detailed drawings of the three probes are shown in Figs. 2.8, 2.9, and 2.10. In the three probes different cone angles are used to expand and slow the flow. The cone angles used in the probes are 3.3° (McGregor 1), 2.0° (McGregor 2), and 0.0° (McGregor 3). By varying the cone angles, the effect of boundary layer development on particle deposition may be investigated.

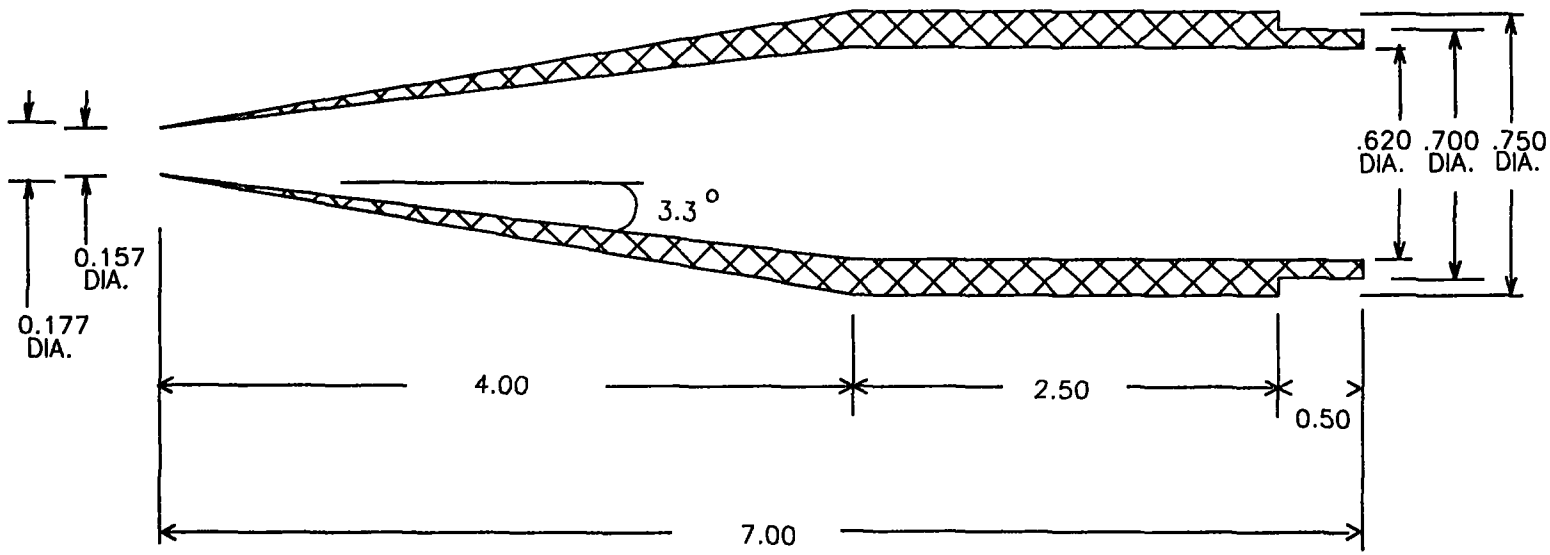

Figure 2.8. Detailed Drawing of McGregor 1 Probe. The Dimension Units are inches and the Tolerances : Length = 0.01 in., Diameter = 0.005 in.

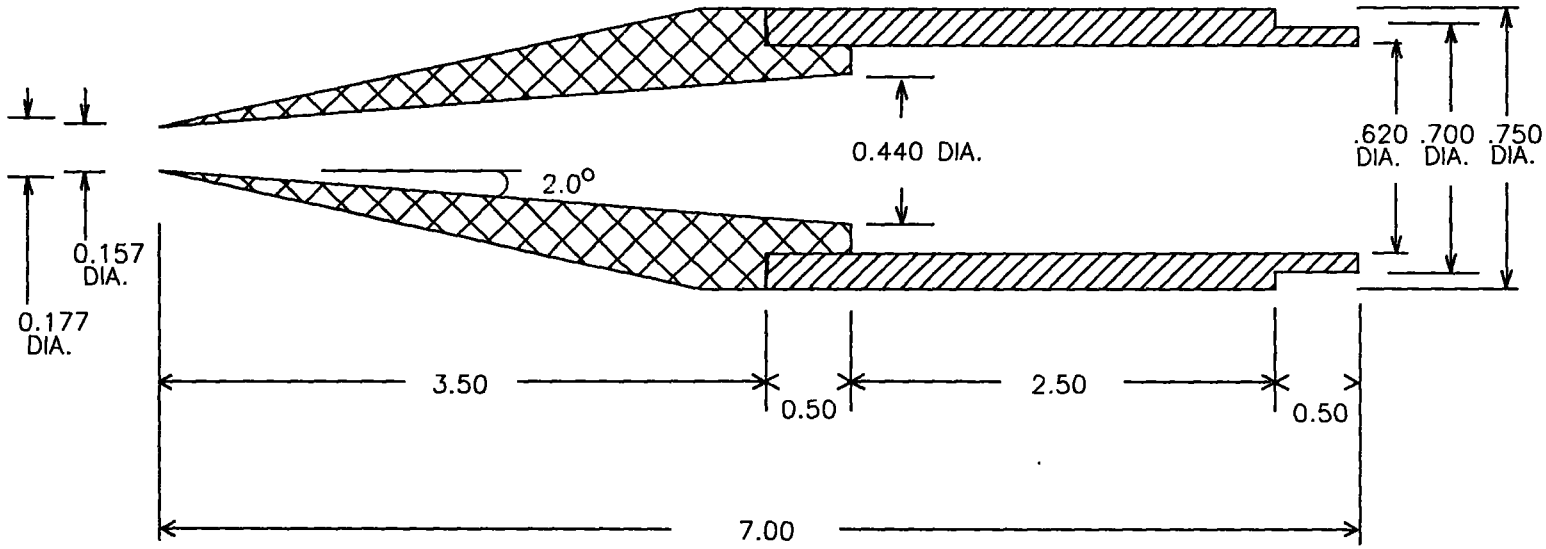

Figure 2.9. Detailed Drawing of McGregor 2 Probe. The Dimension Units are inches and the Tolerances : Length = 0.01 in., Diameter = 0.005 in.

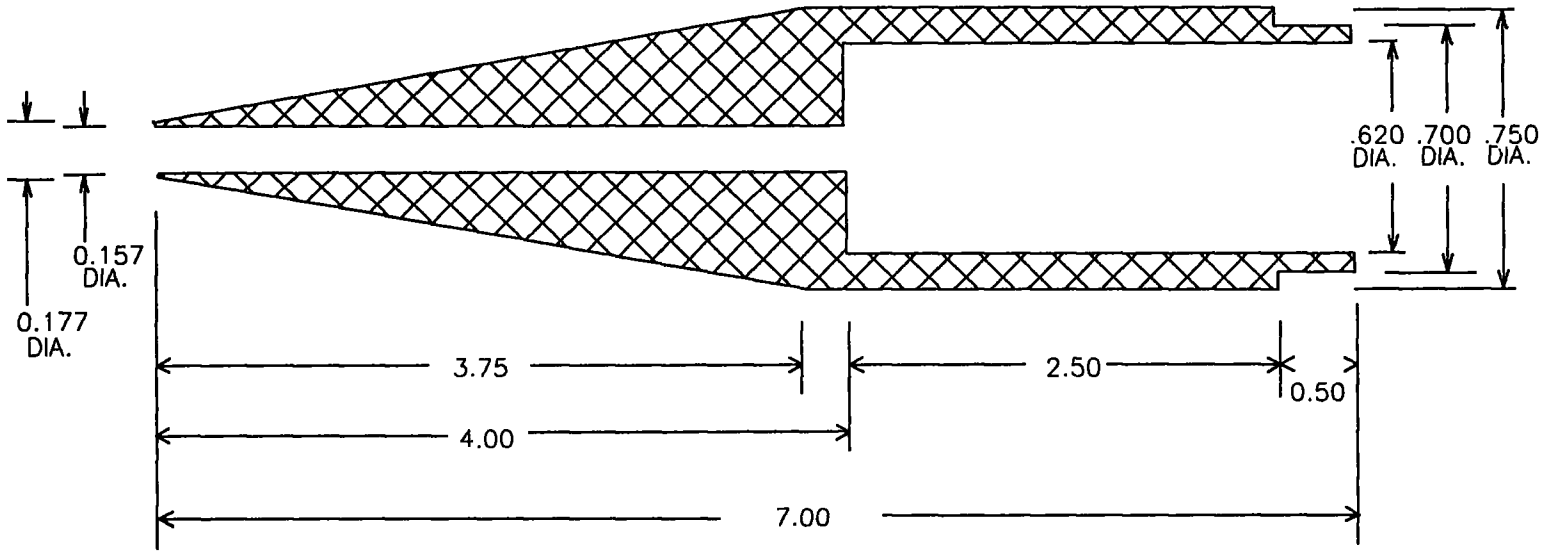

Figure 2.10. Detailed Drawing of McGregor 3 Probe. The Dimension Units are inches and the Tolerances : Length = 0.01 in., Diameter = 0.005 in.

3.0 DIMENSIONAL ANALYSIS

To correctly simulate the factors that lead to the internal wall losses of particles in the probes, the experimental conditions are scaled to the conditions that occur where the probes are used. Table 3.1 shows some of the conditions that are present in the plumes of rocket and jet engines where the sampling probes are used and the laboratory conditions under which the probes are tested in the present study.

The internal wall losses of the particles are a result of the turbulent transport and deposition of particles within the gas recirculating zones of the probes. Because of adverse pressure gradients and thicker boundary layers that cause significant wall separation and gas recirculation, most of the particle wall losses occur near the shock and within the subsonic regions of the probe as shown in Fig. 3.1. As a consequence of the thin boundary layers in the supersonic region, deposition losses are minimal in this section. With these factors in mind, the particle loss E within the probe is a function of the probe geometry, sample tube length, gas Reynolds number, and particle Stokes number evaluated at the conditions found after the shock. Therefore, E can be represented by [9,10,11,12,13]:

$$E = E(\psi, Re, d/D, L/d, L_T/D) \qquad (3.1)$$

where ψ = particle Stokes number (St)

Re = gas Reynolds number

d = probe diameter

TABLE 3.1

FLOW CONDITIONS IN ROCKET PLUME, JET EXHAUST, AND LABORATORY FLOW FOUND AT THE ENTRANCE OF THE SAMPLING PROBES

	Rocket Plume	Jet Exhaust	Laboratory
Mach Number	4.0	1.4	2.5
Heat Capacity Ratio	1.16	1.4	1.4
Speed of Sound (m/s)	760	620	228
Gas Velocity (m/s)	3050	862	569
Stagnation Temperature (K)	3420	1310	293
Stagnation Pressure (psia)	590	60	14.7
Gas Density (g/cc)	2.1×10^{-4}	4.8×10^{-4}	1.5×10^{-4}
Particle Density (g/cc)	4.0	1.0	1.0
Particle Diameter (μm)	0.2-1.0	0.5-1.0	1.0-2.5

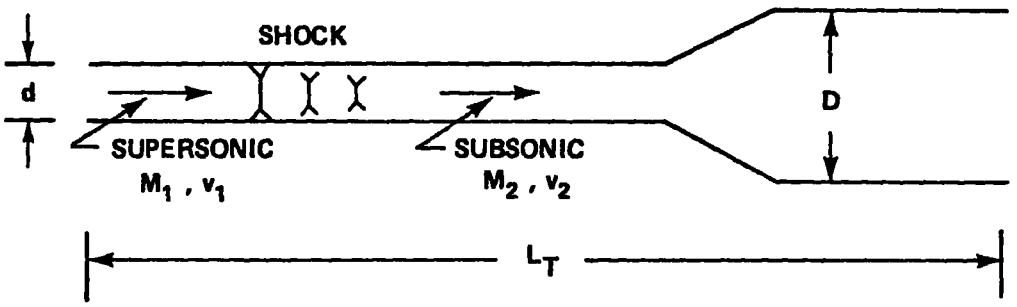

Figure 3.1. Schematic of Supersonic Particle Probe.

D = sample line diameter

L = length of probe

L_T = length of probe including sample line

From the previous section on the probe design, the geometric similarities are built into each of the probes to be tested. Therefore, the remainder of this section focuses on simulating the Reynolds and Stokes numbers that occur in the engine environments. Also, the boundary layer thickness which is related to the Reynolds number is calculated for the probes. Thicker boundary layers in which the particles are able to penetrate could possibly lead to more wall losses.

3.1 REYNOLDS AND STOKES NUMBERS

To experimentally simulate the conditions found in the engine tests, the cold flow experiments are designed to produce similar Stokes and Reynolds numbers [2,14]. The Stokes number, which is the ratio of the particle stopping distance to a probe diameter may be expressed [15]:

$$\psi = \psi_s \phi_c \phi_r \tag{3.2}$$

where ψ_s is the Stokes number based on Stokesian drag, ϕ_c is the Cunningham slip correction factor, and ϕ_r is the non-Stokesian correction factor. Because of the low gas densities and the large particle Reynolds numbers, the correction factors are needed to obtain the proper Stokes number.

In manipulating the Stokes number, the dimensionless group can be expressed as a function of the particle diameter, particle density, gas stagnation conditions before the shock, and the Mach number of the system which are all known

properties. The Stokes number for a particle traveling through a shock assuming Stokesian drag takes the form:

$$\psi_s = \frac{\rho_p M_1 c_1 d_p^2}{9 \mu_2 d} \tag{3.3}$$

where ρ_p = particle diameter (cm)

M_1 = Mach number before shock

c_1 = speed of sound before shock (cm/s)

d_p = particle diameter (cm)

μ_2 = gas viscosity after shock (g/cm s)

d = probe diameter (cm)

Using the following expressions for viscosity and velocity [2,15]:

$$\mu_2 = \mu_{o1} (T_2/T_{o1})^{.5} \tag{3.4}$$

$$c_1 = (\gamma R T_1)^{.5} \tag{3.5}$$

where μ_{o1} = gas viscosity at stagnation conditions

T_2 = gas temperature after shock

T_{o1} = stagnation gas temperature

v_1 = gas velocity before shock

γ = ratio of specific heats

R = gas constant

T_1 = gas temperature before shock

the parameter, ψ_s, takes the form [15]:

$$\psi_s = \frac{\rho_p \, d_p^2 \, M_1 \, c_{o1} \, (T_1/T_2)^{.5}}{9 \, \mu_{o1} \, d} \tag{3.6}$$

where $c_{o1} = (\gamma R T_{o1})^{1/2}$ is the speed of sound in the stagnation reservoir.

In place of the temperature ratio in Eq. 3.6, the normal shock relationship [16]:

$$\frac{T_2}{T_1} = \frac{\left[1 + \frac{\gamma-1}{2} M_1^2\right]\left[\frac{2\gamma}{\gamma-1} M_1^2 - 1\right]}{\frac{(\gamma+1)^2}{2(\gamma-1)} M_1^2} \qquad (3.7)$$

may be used. By substituting Eq. 3.7 into Equation 3.6, ψ_s becomes a function of known properties (particle and stagnation properties, and the Mach number).

The Cunningham slip factor, ϕ_c, is used to correct the ψ_s for any departures from continuum flow caused by the low gas densities. The parameter ϕ_c takes the form [17]:

$$\phi_c = 1 + 2Kn_{o2}(1.257 + 0.4\exp(-0.55/Kn_{o2})) \qquad (3.8)$$

where Kn_{o2} is the Knudsen number based on stagnation conditions after the shock. The Knudsen number which is the ratio of the mean free path of the gas to the diameter of the particle may be expressed [2,15]:

$$Kn_{o2} = (\pi\gamma/2)^{.5}(\mu_{o2}/c_{o2}d_p\rho_{o1})(\rho_{o1}/\rho_{o2}) \qquad (3.9)$$

Because the stagnation temperature does not change across the shock, μ_{o1} and c_{o1} may be substituted for their after shock values in Eq. 3.8. Also by substituting the normal shock relation [16]:

$$\frac{\rho_{o1}}{\rho_{o2}} = \left[\frac{(\gamma+1)M_1^2}{(\gamma-1)M_1^2+2}\right]^{\frac{-\gamma}{\gamma-1}}\left[\frac{\gamma+1}{2\gamma M_1^2-(\gamma-1)}\right]^{\frac{-1}{\gamma-1}} \qquad (3.10)$$

the parameter ϕ_c may be expressed as a function of known properties.

The non-Stokesian correction factor, ϕ_r, is needed because of the large particle velocities found in the system. Consequently, the particle Reynolds numbers are above the limit for which Stokes drag may be assumed. Therefore, the parameter ϕ_r is introduced to correct for the non-Stokesian effects. The parameter takes the form [15,18]:

$$\phi_r = 18/Rep_{o2}(Rep_{o2}^{1/3}-2.52\tan^{-1}(Rep_{o2}^{1/3}/2.52)) \qquad (3.11)$$

where Rep_{o2} is the particle Reynolds number evaluated at the stagnation conditions after the shock [2,15]:

$$Rep_{o2} = \frac{\rho_{o1}M_1c_{o1}\left(T_1/T_{oI}\right)^{.5}(\rho_{o2}/\rho_{o1})}{\mu_{o1}} \qquad (3.12)$$

By substituting Eq. 3.10 and the following isentropic expression for the temperature ratio [16]:

$$\frac{T_{o1}}{T_1} = 1 + \frac{\gamma-1}{2} M_1^2 \qquad (3.13)$$

into Eq. 3.11, the parameter ϕ_r may be expressed as a function of the known factors. Therefore by substituting Eqs. 3.6, 3.8, and 3.11 into Eq. 3.2, the corrected Stokes number ψ may be calculated.

Similar to the Stokes number, the probe Reynolds number (Re) may be calculated from stagnation gas and particle properties. The Reynolds number becomes [2,15]:

$$Re = \frac{M_2c_{o1}d(\rho_2/\rho_{o1})}{\nu_{o1}} \qquad (3.14)$$

where M_2 = Mach number after shock

ν_{o1} = kinematic viscosity at stagnation conditions

ρ_2 = gas density after shock.

By substituting in the normal shock expression for the density ratio [16]:

$$\frac{\rho_2}{\rho_{o1}} = \frac{(\gamma+1)M_1^2}{(\gamma-1)M_1^2+2}\left[1+\frac{\gamma-1}{2}M_1^2\right]^{-1/(\gamma-1)} \qquad (3.15)$$

the Reynolds number may be calculated from the known data. Now with the expressions developed, a comparison between the laboratory and actual engine conditions may be made.

A comparison of the important dimensionless groups for the engine and laboratory tests are given in Table 3.2. As shown the laboratory values of Re and St are the same order of magnitude as the rocket and jet engine values. The laboratory experiments using the larger diameter particles should be applicable to the rocket plume case, while the smaller particle experiments should be applicable to the jet engine case.

The last row in Table 3.2 is a dimensionless group developed by Willeke et. al. [19] that relates the particle inertia (Stokes number) to the growth of the boundary layer ($1/Re^{.5}$). Willeke used this group to correlate the deposition rates in the entrance section of ducts. Referring to Fig. 3.2, the particle is assumed to deposit if it penetrates the boundary layer. If the Reynolds number is low, the boundary layer grows rapidly. Therefore, particles with large Stokes numbers (high inertia) will penetrate the boundary layer and deposit. If the Reynolds number is high, the boundary layer stays thin and the particles will project past the boundary layer staying in the core flow. As seen in Table 3.2, the parameters $St/Re^{.5}$ for the three cases are comparable.

TABLE 3.2

Dimensionless Groups Important in Deposition

	Rocket	Jet	Laboratory
$d_p(\mu m)$	0.1 ↔ 1.0	0.1 ↔ 1.0	1.0 ↔ 2.5
d (cm)	2.54	0.4	0.4
M_1	4.0	1.4	2.5
M_2	0.35	0.74	0.51
Rep_{o2}	0.76 ↔ 7.6	0.38 ↔ 3.8	18.6 ↔ 46.5
Kn_{o2}	6.3 ↔ 0.63	1.1 ↔ 0.11	0.11 ↔ 0.05
Re	$1.8x10^4$	$3.6x10^4$	$2.0x10^4$
St(ψ)	0.60 ↔ 6.3	0.023 ↔ 0.43	0.44 ↔ 2.8
$St/Re^{0.5}$	$4.5 \leftrightarrow 47x10^{-3}$	$0.12 \leftrightarrow 2.3x10^{-3}$	$2.3 \leftrightarrow 20x10^{-3}$

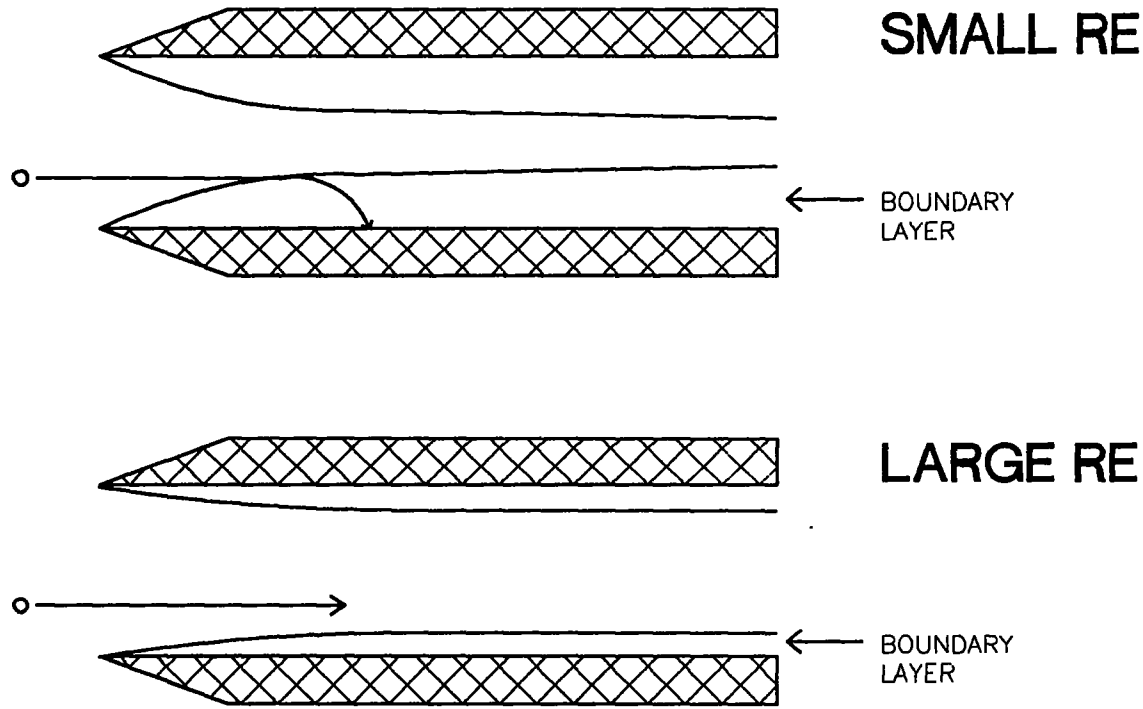

Figure 3.2. Boundary Layer Growth and Particle Deposition. At Smaller Re, Larger Boundary Layers lead to more Deposition and vice versa.

3.2 BOUNDARY LAYER GROWTH

Since the growth of the boundary layer has a significant effect on deposition [10,18,20,21] the boundary layer thickness for the McGregor 1, 2, and 3 probes and the Colket 1 probe is estimated. The boundary layers in the Dehne probes should be similar in the supersonic section to the Colket 1 probe while comparable to the McGregor 3 probe in the subsonic section. To estimate the boundary layer thickness, the developing boundary layer in the cylindrical probes is assumed to be similar to that of a flat plate. This assumption is valid as long as the thickness of the boundary layer is much smaller than the radius of the probe [22]. Initially, a laminar boundary layer exists that changes to a turbulent boundary layer when the Reynolds number (Re_x) based on duct length reaches 5×10^5 [22]. For the laminar boundary layer, the boundary layer thickness may be calculated [22]:

$$\delta/x = A/Re_x^{.5} \qquad Re_x < 5 \times 10^5 \qquad (3.16)$$

where δ = boundary layer thickness

x = distance from probe entrance

$A = 5.0\exp(0.1M^{1.5})$

Re_x = Reynolds number based on duct length

M = Mach number in probe.

The coefficient A is used to account for compressibility effects and was fitted from data taken by Crocco [23] reported by Schlichting [22] assuming an adiabatic flat plate. As the Mach number of the free stream increases, the relative thickness of the boundary layer increases because of the temperature rise in the boundary layer.

In the transition to a turbulent boundary layer the boundary layer increases in thickness. The eddy diffusion between the layers of fluid in the turbulent boundary layer is theorized to be a mechanism of particle deposition [10,17]. The thickness of the turbulent boundary layer may be estimated [22]:

$$\delta/x = 6.4C_f \qquad Re_x > 5 \times 10^5 \qquad (3.17)$$

where C_f is the local skin friction coefficient. The local skin friction coefficient may be estimated [22]:

$$C_f = (2\log(Re_x) - .65)^{-2.3}/2 \qquad (3.18)$$

The effect of high Mach numbers in the turbulent boundary layer causes the skin friction to decrease. On the other hand the temperature in the boundary layer increases, therefore the two effects cancel each other over the range of Mach number found in the present study.

Figures 3.3, 3.4, 3.5, and 3.6 show the calculated boundary layers in the McGregor probes and the Colket 1 probe. In Figs. 3.3 and 3.4, a laminar boundary layer exists up to x/L=0.075 in McGregor 1 and up to x/L=0.125 in McGregor 2 [24,25]. At these points the boundary layer separates and becomes turbulent as a result of the adverse pressure gradient caused by the flow deceleration. Though the particles are not deeply projected into the boundary layer, experiments performed on subsonic diffusers show that areas of stall (turbulent boundary layer separation and gas recirculation) are present in McGregor 1 while not in McGregor 2 [24]. These areas of stall could lead to increased deposition. Interestingly, the 2° half angle used in the McGregor 2 probe is approximately the angle needed to prevent particle penetration into the boundary layer. By not allowing the

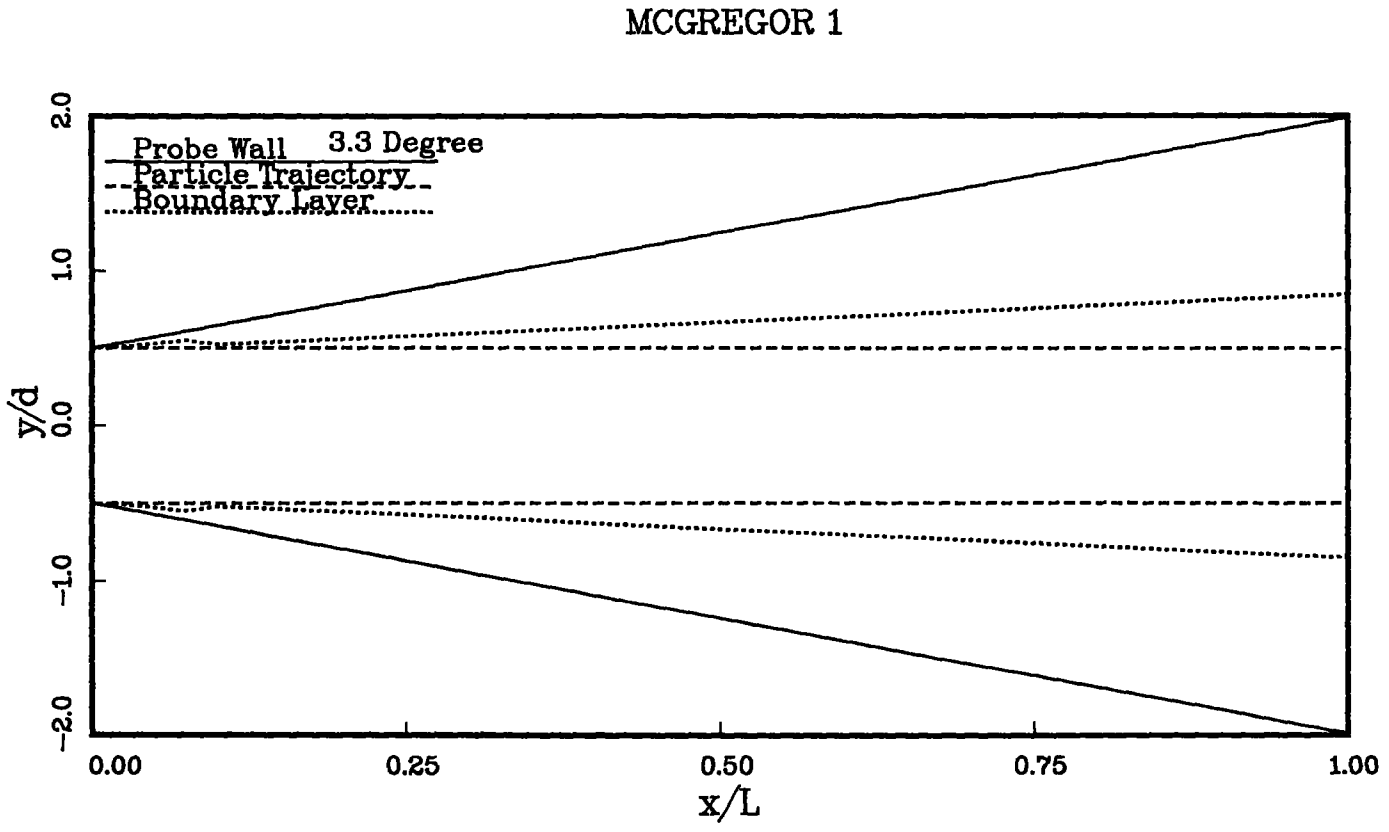

Figure 3.3 Boundary Layer Development in the McGregor 1 Probe.

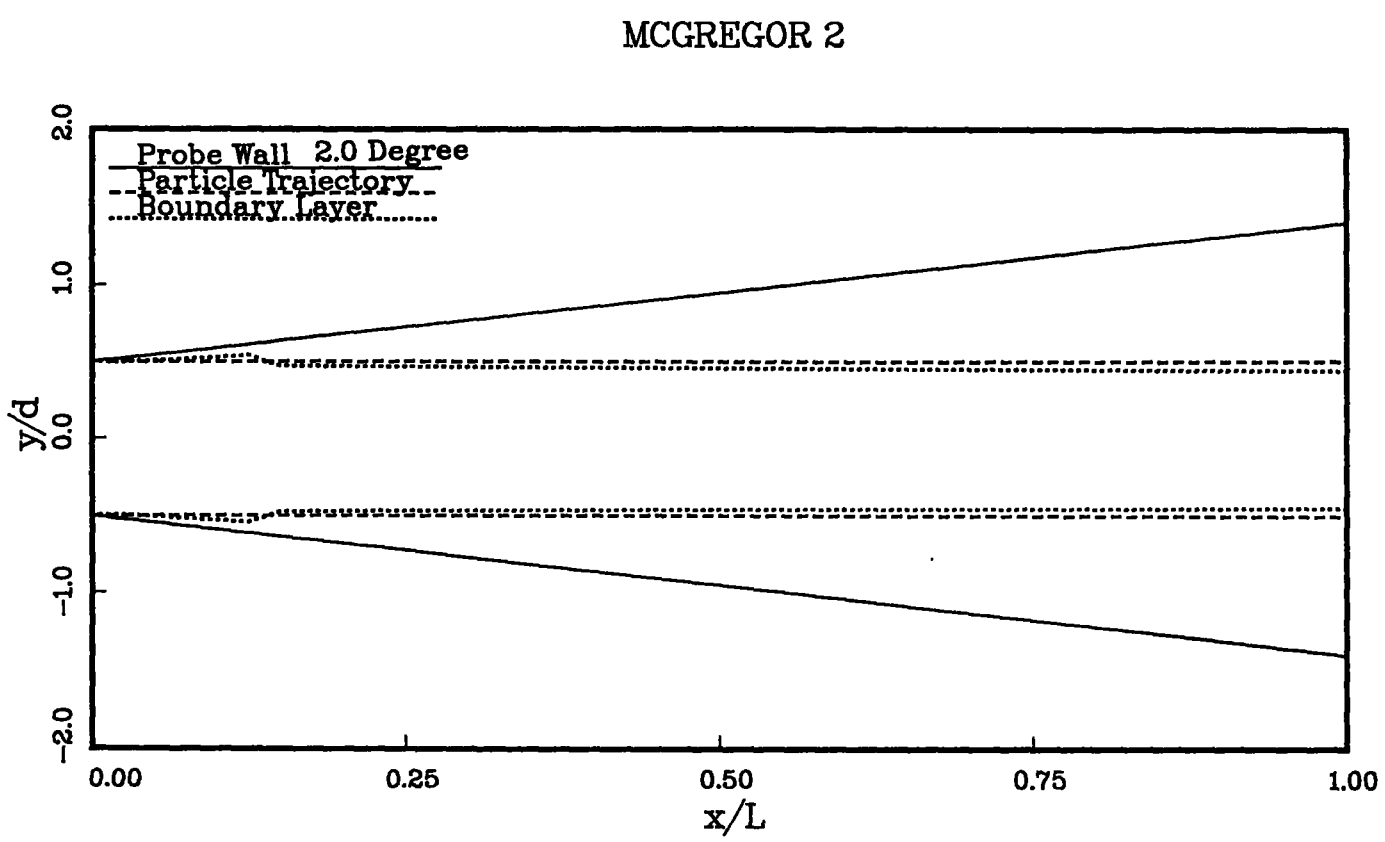

Figure 3.4 Boundary Layer Development in the McGregor 2 Probe.

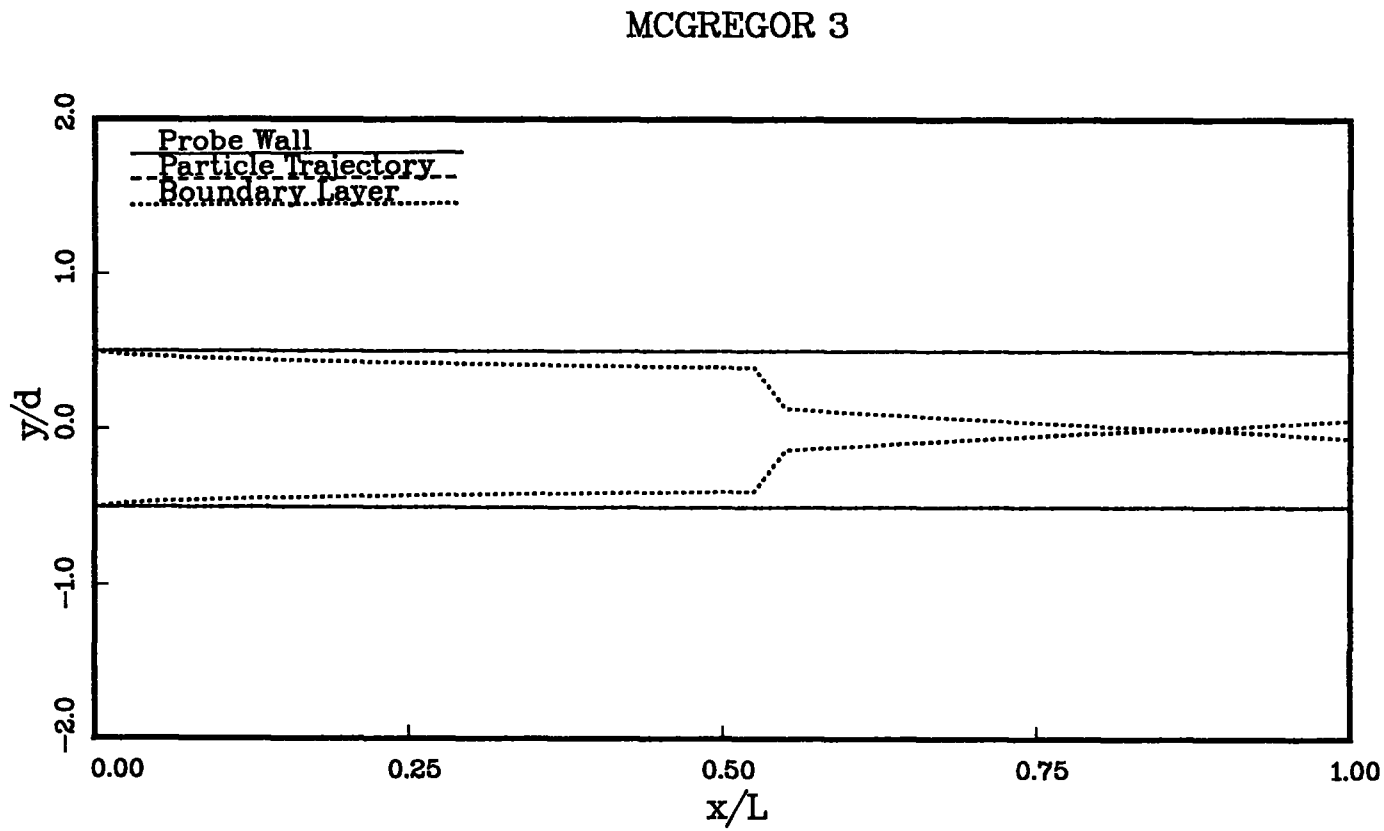

Figure 3.5 Boundary Layer Development in the McGregor 3 Probe.

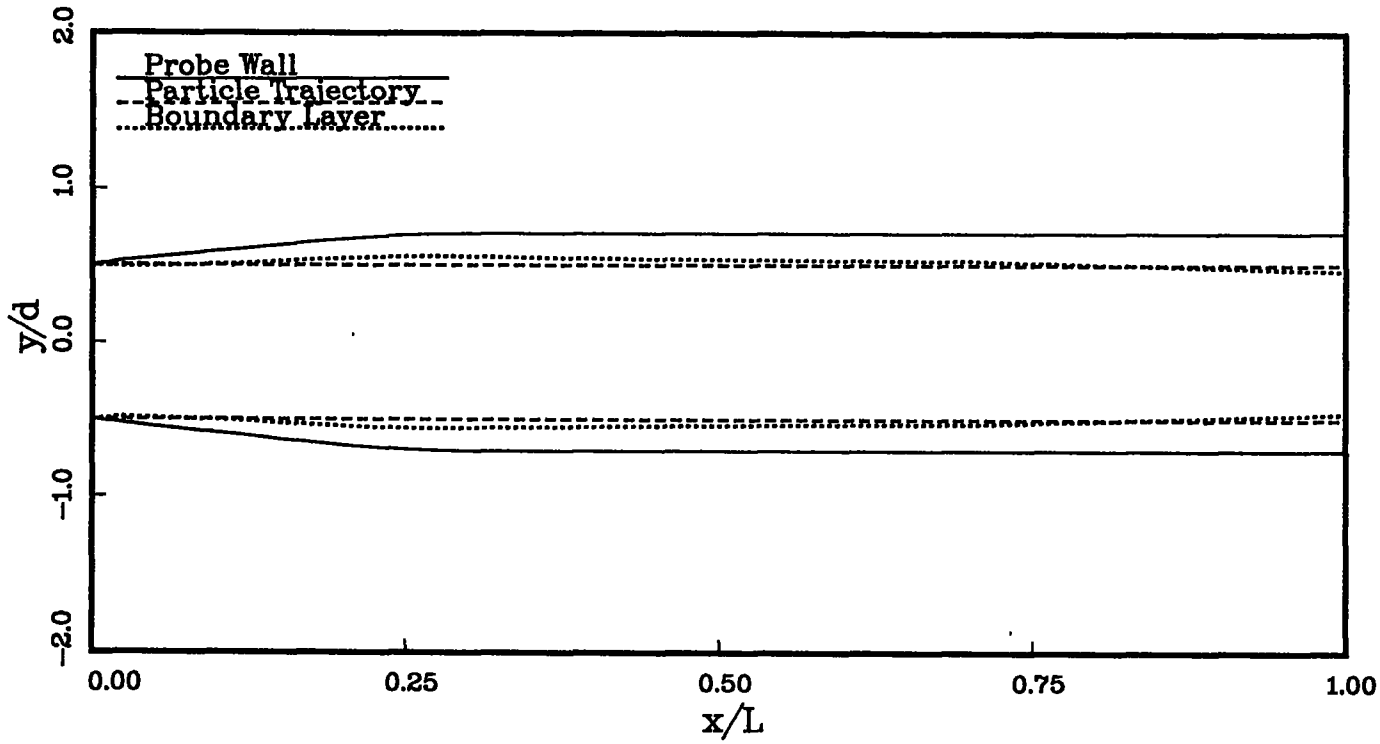

Figure 3.6 Boundary Layer Development in the Colket 1 Probe.

particles to enter the boundary layer, less deposition should occur.

Figure 3.5 shows the boundary layer development in the McGregor 3 probe. In this case the particle trajectory and probe wall coincide. Unlike McGregor 1 and 2, no adverse pressure gradient is present to cause separation. The transition from a laminar to a turbulent boundary layer occurs at x/L=0.55 and is caused by an instability indicated by a high Re_x (5×10^5). As shown in Fig. 3.5, the particles that enter the probe are able to penetrate into the boundary layer. Because the boundary layer is not pulled away from the particle trajectories as in McGregor 1 and 2, increased deposition should occur in McGregor 3.

Figure 3.6 shows the boundary layer development in the Colket 1 probe. The transition from a laminar to a turbulent boundary layer occurs at x/L=0.70 and is again caused by instability indicated by a high Re_x. For the majority of the probe, the particle trajectories are outside of the boundary layer. Separation of the boundary layer is a possiblity because of the adverse pressure gradient in the constant area throat. Because of the supersonic speeds, the frictional choking causes the velocity to decrease and the pressure to rise as the flow passes through the throat. As mentioned before, the separation of the boundary layer could lead to increased deposition.

In Appendix B, an example of the computer program used to calculate the boundary layers is given.

4.0 EQUIPMENT AND PROCEDURE

The essential components of the experimental apparatus were an aerosol generator to produce mono sized droplets, a probe test section that accelerates the drop-laden gas to supersonic speeds, and a monitoring system to determine probe deposition rates, pressures, and flow rates. Below, a description of each of these elements and the experimental procedure is given.

4.1 AEROSOL GENERATOR

The test aerosol for the probe sampling experiments was monosized dioctylphathalate (DOP) oil droplets. To prevent any particle bounce from the internal probe surfaces, oil droplets were used. The aerosols in 1.0, 1.5, 2.0, and 2.5 micron sizes were generated with a Berglund-Liu vibrating orifice aerosol generator (TSI Model 3450). The aerosol generation system is pictured in Fig. 4.1 [26].

Referring to Fig. 4.1, a mixture of ethanol/DOP was filtered and fed to the drop generation assembly by a syringe pump. The pressure in the liquid feed line was monitored and a bypass (drain valve) was provided in the event the orifice of the generator became obstructed. Also two clean, dehumidified air streams were fed to the drop generation assembly. The dispersion air stream was used to prevent droplet coagulation as the drops were formed by the vibrating action of the orifice. With the other air stream (dilution air), the droplets were entrained upward through a drying column where the ethanol in the drops evaporated leaving the DOP. One final input to the droplet generation assembly was an electrical signal from a signal generator

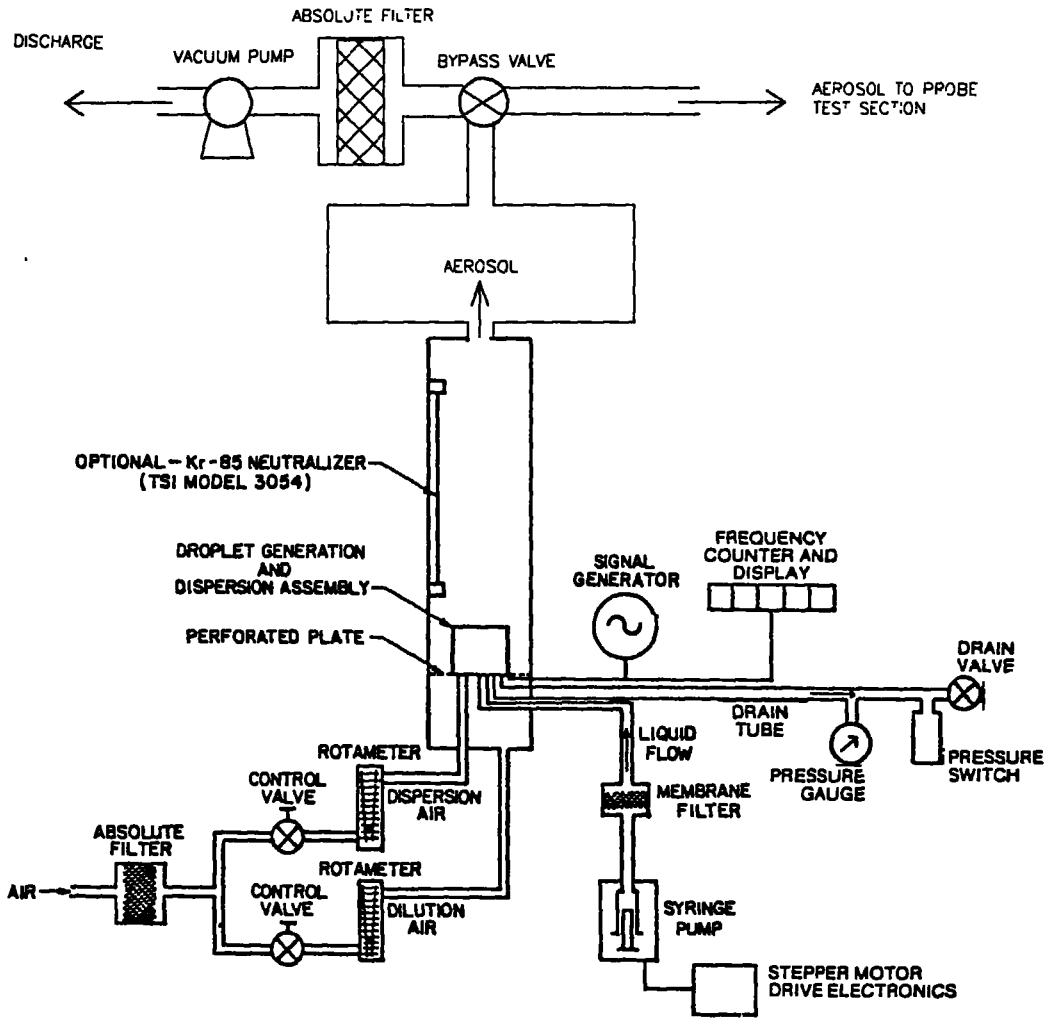

Figure 4.1. Aerosol Generation System.

that caused the housing (piezoelectric ceramic) of the orifice to vibrate. Therefore, by direct contact the orifice vibrated. By manipulating the orifice vibration frequency, stable monosized droplets were produced [26].

To produce the various droplet sizes, different dilution factors of DOP to ethanol were fed through the orifice. Table 4.1 shows the important operating parameters for the drop generator.

Table 4.1

Operating Parameters for Aerosol Generator

Drop Sizes (μm)	1.0	1.5	2.0	2.5
Dilution Factor (ml DOP:ml Ethanol)	1:5000	1:2500	1:1000	1:500

(These parameters were same for all drop sizes)

Orifice Frequency (kHz)	155
Liquid Flow Rate (cc/min)	0.080
Orifice Diameter (microns)	10
Dilution Air Flow Rate (l/min)	50
Dispersion Air Flow Rate (l/min)	1.5

During the time the droplets travel up the drying column, the drops were exposed to a Kr-85 neutralizer (TSI Model 3054) that removed any static charge from the particles [27]. Finally, after leaving the drying column, the drops were sent to a holding chamber. From the holding chamber the drops were sent to the probe test section where they were exposed to the probe or they were sent to a bypass filter which removed the droplets before discharging the air.

4.2 PROBE TEST SECTION

The probe test section consisted of an entrance chamber, a supersonic converging-diverging nozzle, the particle probe,

discharge ducting, and vacuum tank. Fig. 4.2 shows the probe test section.

Referring to Fig. 4.2, the entrance chamber consisted of a plexiglas box that funnels the drops from the holding chamber to the mouth of the supersonic nozzle. The supersonic nozzle was constructed of plexiglas and had a throat diameter of 0.53 in. The nozzle had an exit plane to throat area ratio of 4.25 allowing for theoretical flow rates up to Mach 3.0 [16]. Immediately downstream of the nozzle, the particle probe was suspended in a piece of 3.0 in. plexiglas pipe by an adjustable mounting screw (not shown). By allowing the probe to traverse horizontally the mouth of the probe was positioned within the nozzle where the drop-laden stream was traveling at Mach 2.5. Though the particle velocity lagged behind the accelerating gas velocity, calculations performed in Appendix B showed that the particle velocity was within 95% of the gas velocity. Not shown in Fig. 4.2, pressure taps from the sampling probe were run through the discharge ducting wall using a combination of 1/16 in. diameter rigid and flexible tubing. The taps were connected to mercury-filled U-tube manometers so that pressures within the sampling probes were monitored.

After the supersonic nozzle the gas not swallowed by the probe was carried by 3.0 in. copper tubing to a vacuum tank. The 3.0 in. gate valve shown in Fig. 4.2 was used to start and stop the flow to the vacuum tank. The vacuum tank had a volume of 1650 ft^3 and could be evacuated to a pressure of 28in. of Hg vacuum. The gas sample swallowed by the probe passed through a 30 in. long piece of 3/4 in. tubing before entering the filter shown in Fig. 4.3.

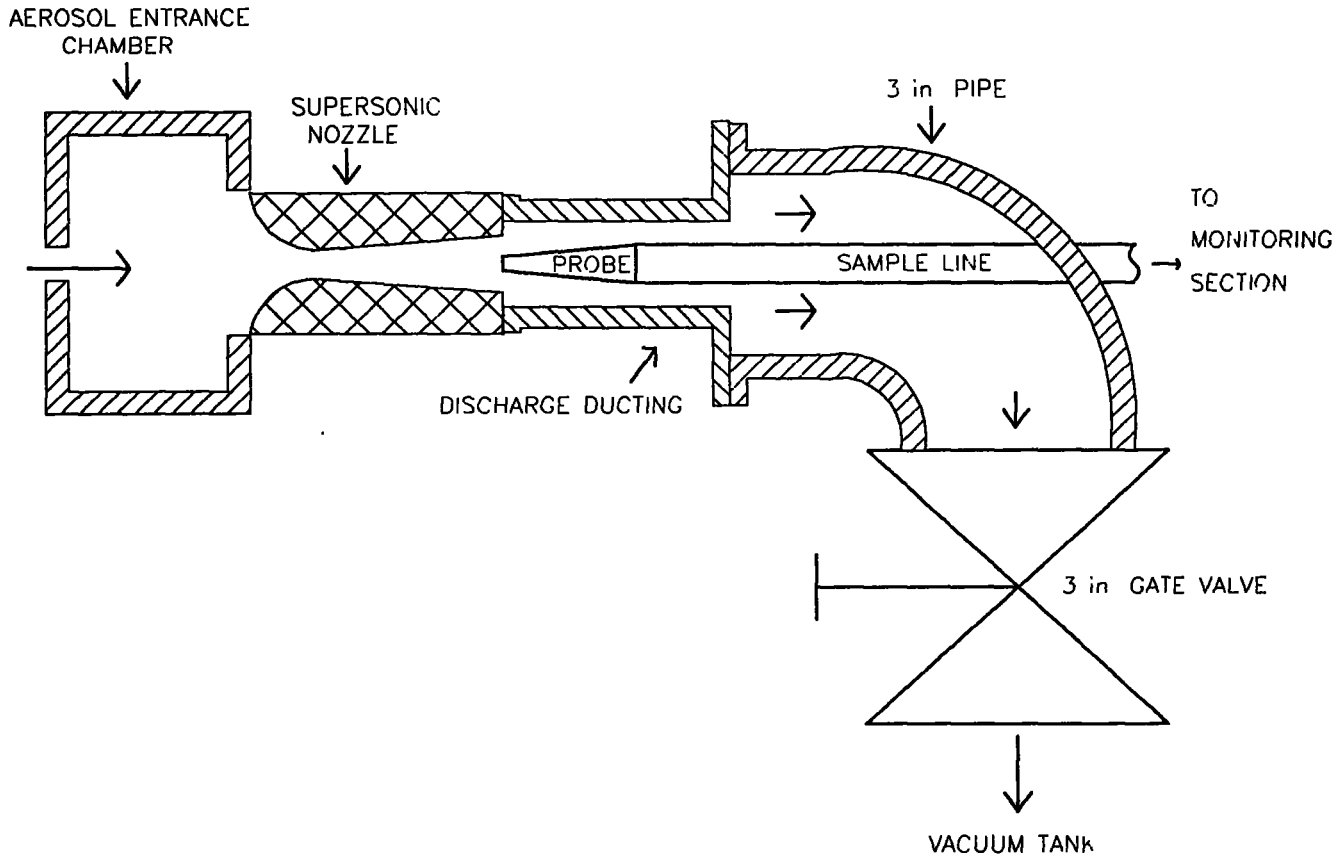

Figure 4.2. Probe Test Section.

4.3 MONITORING SYSTEM

Most of the flow rate and particle measurements were done on the gas stream coming from the probe. Figure 4.3 shows the orientation of the equipment used to make the necessary measurements.

The gas and particles that were swallowed by the probe traveled through a 3/4 in. diameter sample line to a filter. The filter consisted of a 4.0 in. disc of glass fiber filter paper wedged between two 6.0 in. long pieces of 3.5 in. diameter plexiglas pipe. The paper (Model FP4.0M) was manufactured by Miami Air Sampler Company and was noted for its high collection efficiency (98%+) and low pressure drop characteristics.

After the filter, the gas stream was passed through a 1/2 in. gate valve that was used to control the flow rate swallowed by the probe. Then after the valve, the stream went through a Hastings flowmeter (Model AFSC-50K) to obtain the mass flow rate of gas passed through the probe. This flowmeter used the heat transfer rate from a heating element to measure the mass flow rate of the stream. Since the heat transfer rate was proportional to the mass flow rate, no temperature or pressure compensation was required.

From the flowmeter the stream then went through a 3/4 in. ball valve that was used as an on/off valve to isolate the system from the vacuum tank. After the ball valve, the stream was piped to the vacuum tank.

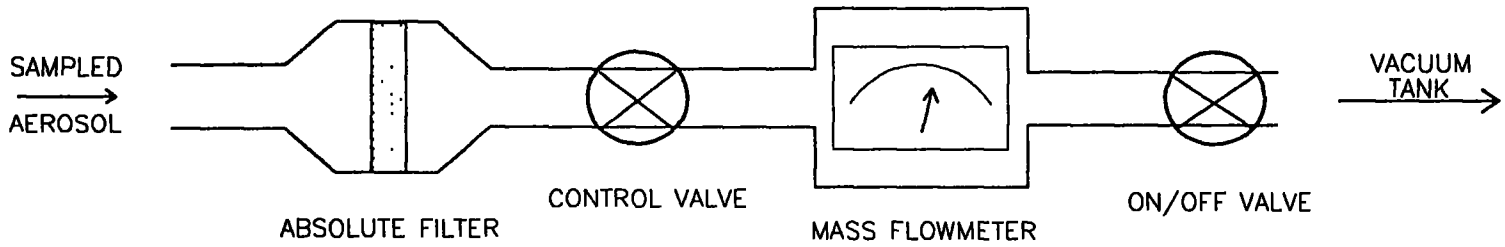

Figure 4.3. Monitoring Section.

4.4 EXPERIMENTAL PROCEDURE

To begin the deposition measurements, the aerosol generator was operated for several minutes to reach equilibrium output of approximately 10^5 particles/sec. Special care was taken to ensure that these particles were of a fixed, monosized diameter. To verify the particle diameter, a sample was impacted onto a glass microscope slide. Using a microscope to measure the particles and knowing the spreading factor for DOP [28], the actual particle diameter could be confirmed. As the aerosol generator was warming up, the bypass line from the droplet holding chamber was open so that no DOP droplets were released in the laboratory environment.

While the aerosol generator was warming up, the mouth of the sampling probe to be tested was positioned in the supersonic nozzle at the point where Mach 2.5 occurred. To do this, the flow through the nozzle was started and the probe was moved horizontally within the nozzle like a pitot tube. From the stagnation pressure readings within the probe, sample line, and filter the Mach number at the probe mouth was verified [16]. Also any deviation in the stagnation pressure recorded at the different pressure taps was used to detect any leaks in the ducting downstream of the probe.

After the probe was positioned, flow was started in the probe. In the McGregor probes, the 1/2 in. gate valve was opened fully. After the mass flow rate was recorded at the choked condition, the gate valve was closed reducing the mass flow rate to 95% of its choked value. By reducing the flow rate, the normal shock caused by the presence of the probe was positioned just outside the mouth of the probe [6].

In the Dehne probes, the same procedure was used as in the McGregor probes except that the flow rate was not reduced for its choked value. Instead the pressure readings within the probe were monitored and the 1/2 in. gate valve was used

to manipulate the back pressure so that the shock train was positioned in the constant area throat of the probe.

In the Colket probes, the experimental setup was slightly modified. To run the tests on the Colket probes, the mass flowmeter and the 1/2 in. gate valve were replaced by a 25 in. long piece of 3/4 in. diameter tubing. By removing these items, the low back pressure needed to position the shock at the end of the constant area throat was achieved. The flow in the Colket probes was started by opening the 3/4 in. ball valve. The pressure taps in the probe were monitored to ensure that the shock was located at the correct position. In Appendix B, the pressure data from the probes was compared to the results obtained from a one-dimensional gas dynamic equation which also helped verify the type of flow in each probe.

After flow in the probes was established, the aerosol from the generator was introduced into the entrance chamber located before the supersonic nozzle. The probe was exposed to the drop-laden stream for five minutes before the flows in the probe and in the nozzle were stopped.

After the probe and the nozzle flows were stopped, the internal surfaces of the probe and the filter paper were washed with measured amounts of ethanol. Because a small amount of a fluorescent tracer (uranine) was added to the DOP solution used in the generation of the drops, the amounts of the uranine found on the internal surface and on the filter paper suspended behind the probe were used to measure the deposited and undeposited drops, respectively. From experimental observation, the deposition in the sample line between the probe and filter was found to be less than 1% and therefore ignored. Appendix D has the fluorescence, pressure, and mass flow rate data gathered on all the probes.

5.0 RESULTS AND DISCUSSION

Measurement of the deposition in each probe was made at four particle diameters: 1.0, 1.5, 2.0, and 2.5 μm. From these measurements, the amount of deposition always increased with diameter. Because the larger particles (larger Stokes numbers) were better able to penetrate the boundary layer (see Fig. 3.2), more deposition occurred when larger particles were used. Therefore, the size distribution of particles was biased toward the smaller particles due to the internal wall losses in the probes. The following sections compare and contrast the probe operating characteristics: wall losses, pressure recovery, and ease of operation.

5.1 WALL LOSSES

Deposition measurements were performed on all probes and these results are shown in Figs. 5.1, 5.2, and 5.3. Figure 5.1 shows the wall losses found in the Dehne probes pictured in Figs. 2.2 and 2.3. From the results, Dehne 1 appeared to have less deposition at each drop diameter (1, 1.5, 2.0, 2.5 μm) tested. On average Dehne 1 had 20% less deposition than Dehne 2. The increased deposition seen in Dehne 2 was attributed to the different transitions between the constant area throat and the sample line used in the two probes. The 30° subsonic diffuser used in Dehne 1 reduced the gas recirculation and stagnation zones found in the transition [24,25]. On the other hand, the sudden expansion used in Dehne 2 caused more fluid turbulence and provided more motionless pockets which intensified the deposition.

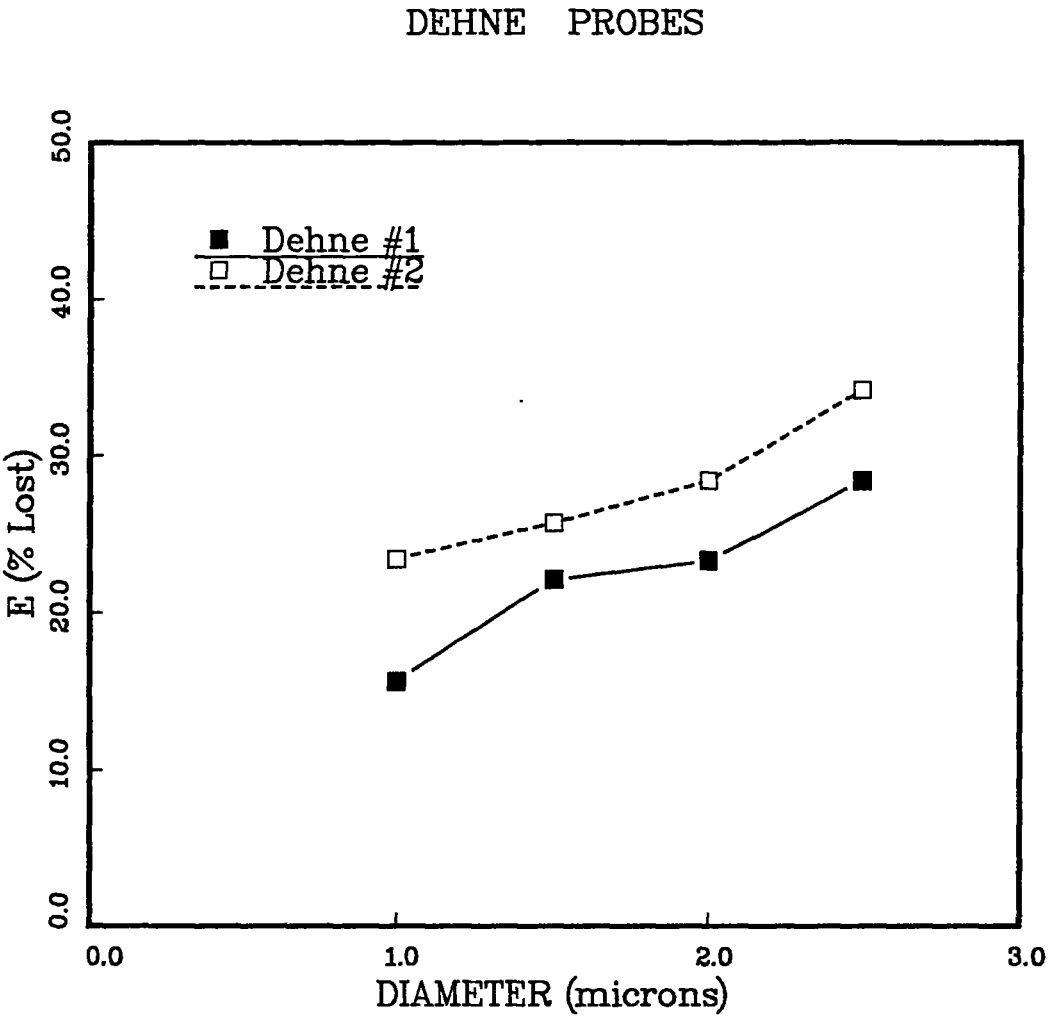

Figure 5.1. Percent of Deposited Particles (E) in the Dehne Probes Versus the Particle Diameter (d_p).

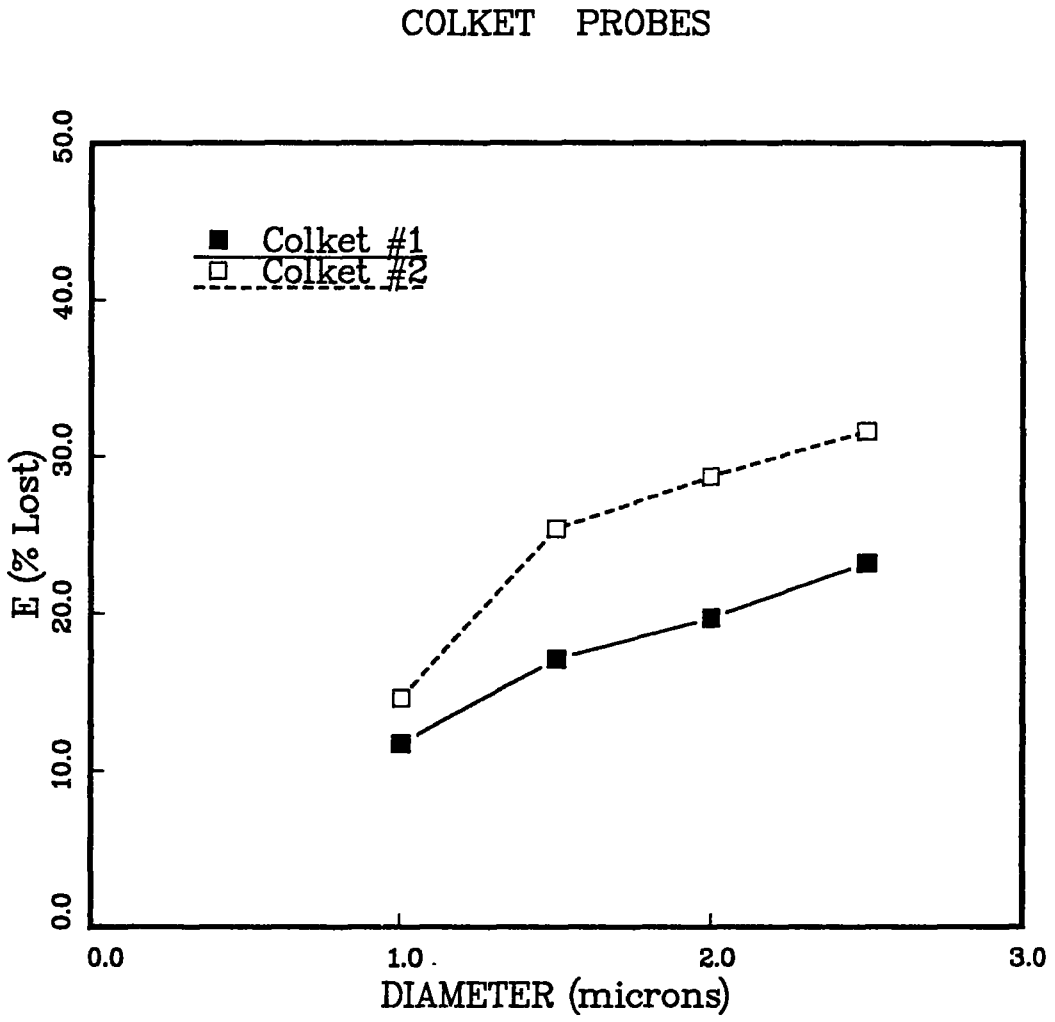

Figure 5.2. Percent of Deposited Particles (E) in the Colket Probes Versus the Particle Diameter (d_p).

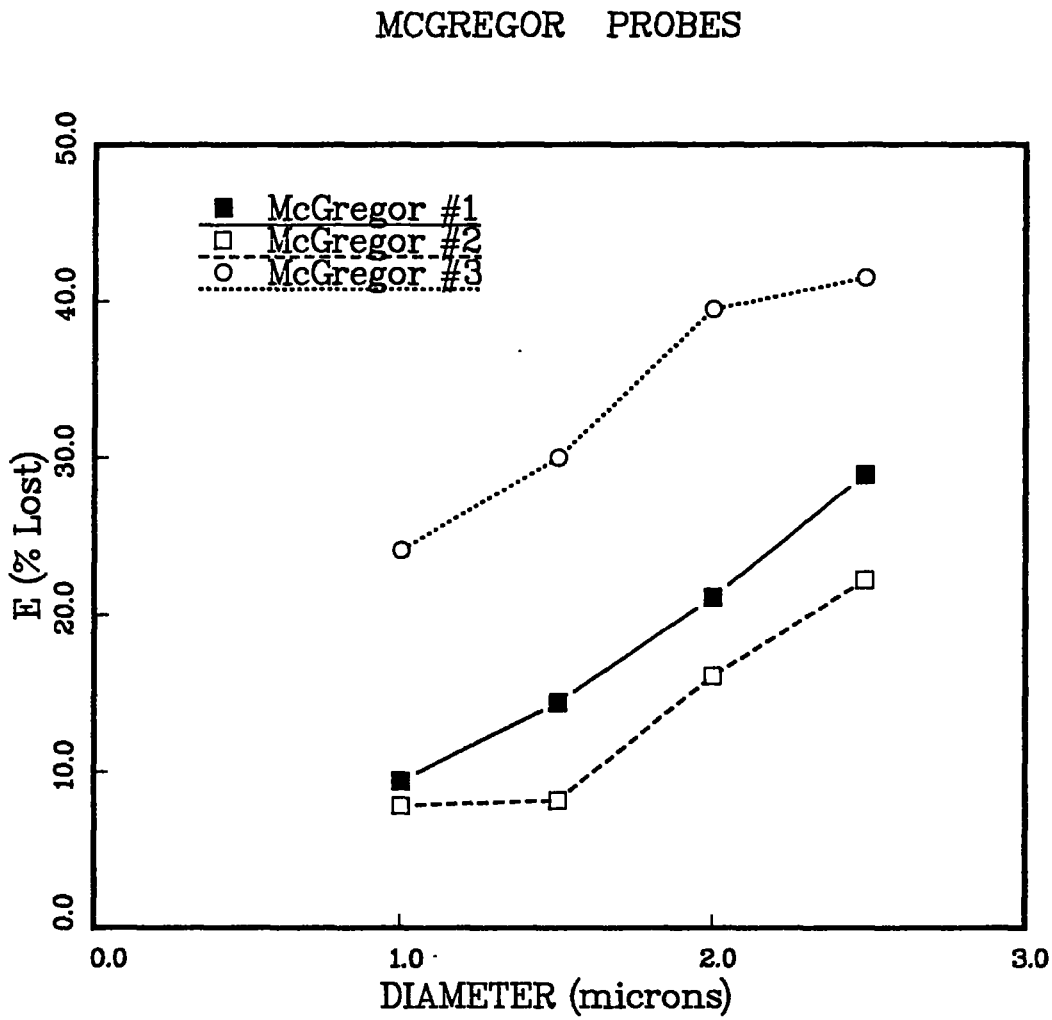

Figure 5.3. Percent of Deposited Particles (E) in the McGregor Probes Versus the Particle Diameter (d_p).

Figure 5.2 shows the results of the deposition measurements performed on the Colket 1 and 2 probes pictured in Figs. 2.5 and 2.6. These results showed that Colket 1 had less internal wall losses at each of the test particle diameters. On average Colket 1 had 28% less deposition than Colket 2. As previously stated, the only difference between the two designs was Colket 2 did not have a supersonic constant area throat. Because of the thin boundary layer in the constant area throat of Colket 1 as shown in Fig. 3.6, less deposition occurred. The subsonic throat of Colket 2 produced larger boundary layers and therefore more internal wall losses.

Another possibility that may have led to the difference was the dissimilar conditions at the sudden expansion of both probes. The shock in Colket 1 happened at the end of the supersonic throat that choked the flow and reduced the Mach number (velocity). In Colket 2, the shock occurred at the end of the supersonic expansion where the maximum Mach number in the probe occurred. Therefore, more recirculation and stagnant areas were present in the Colket 2 probe that produced more deposition.

Figure 5.3 shows the results of the deposition measurements performed on the McGregor probes pictured in Figs. 2.8, 2.9, and 2.10. The deposition results showed that McGregor 3 had twice as much deposition as either McGregor 1 or McGregor 2. Also McGregor 2 was found to have on average 25% less deposition than McGregor 1.

The major difference between the three McGregor probes was the diverging angle of the subsonic diffuser section. In McGregor 3, a 0° diffuser angle (constant area duct) was used. Because the ingested flow was parallel to the probe walls, the particles were projected into the developing boundary layer as pictured in Fig. 3.5. In McGregor 1 and 2, the probe walls diverged carrying the boundary layer away from the particles

as shown in Figs. 3.3 and 3.4. At the probe entrance, the particles were not allowed to flow outwardly to the boundary layer because of their inertia. By using a divergent angle of 2.0°, the McGregor 2 probe employed the optimal angle that prevented particle-boundary layer interaction while also preventing separation of the boundary layer caused by the adverse pressure gradient in the diffuser [24,25]. The 3.3° divergent angle used in the McGregor 3 probe also prevented particle-boundary layer interaction but the adverse pressure gradient was too large resulting in areas of stall that enhanced deposition.

Comparing the particle deposition found in the McGregor probes and the Colket probes, the Dehne probes usually had more wall losses. In the comparison of the best probes from each class shown in Fig. 5.4, the deposition in the Dehne 1 probe averaged 60% greater than the best McGregor probe. The increased deposition in the Dehne probes was blamed on the shock-boundary layer interaction that occurred in the constant area throat of the Dehne probes. Referring to Fig. 5.5, the shock train in the throat of the Dehne probes caused areas of low and high pressure. Because the momentum of the boundary layer was not great enough to overcome the adverse pressuregradients, the boundary layer separated [16,29]. The separation significantly increased the size of the boundary layer and exposed more of the particles to possible deposition. Also with the gas recirculation, the particles were pushed toward the probe wall.

Comparing the particle deposition found in the McGregor probes and the Dehne probes, the Colket 1 probe was one of the best designs to minimize deposition. Only the McGregor 2 probe had less internal deposition as shown in Fig. 5.4. The major reasons for the minimal deposition were the smaller supersonic boundary layer and the decreased Mach number at the shock-inducing expansion of the probe. Furthermore, the decreased

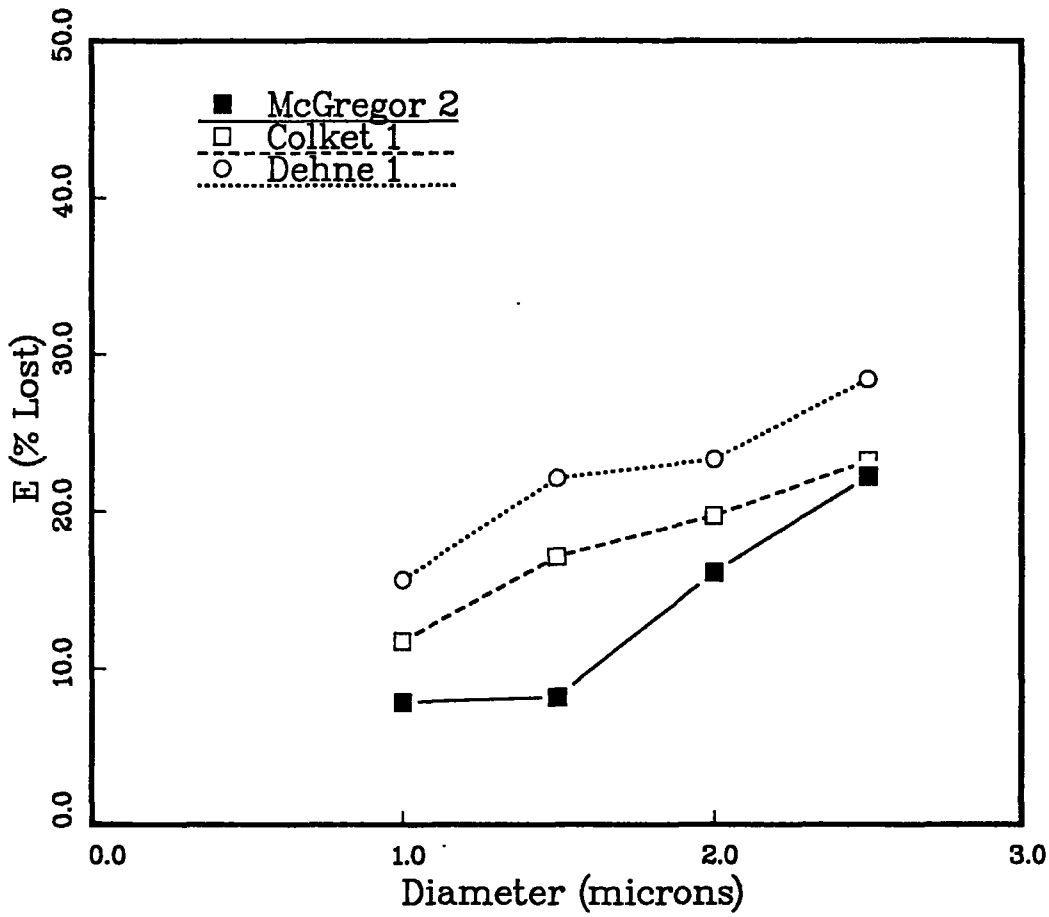

Figure 5.4 Percent of Deposited Particles (E) in the Best from each Design Class versus the Particle Diameter (d_p).

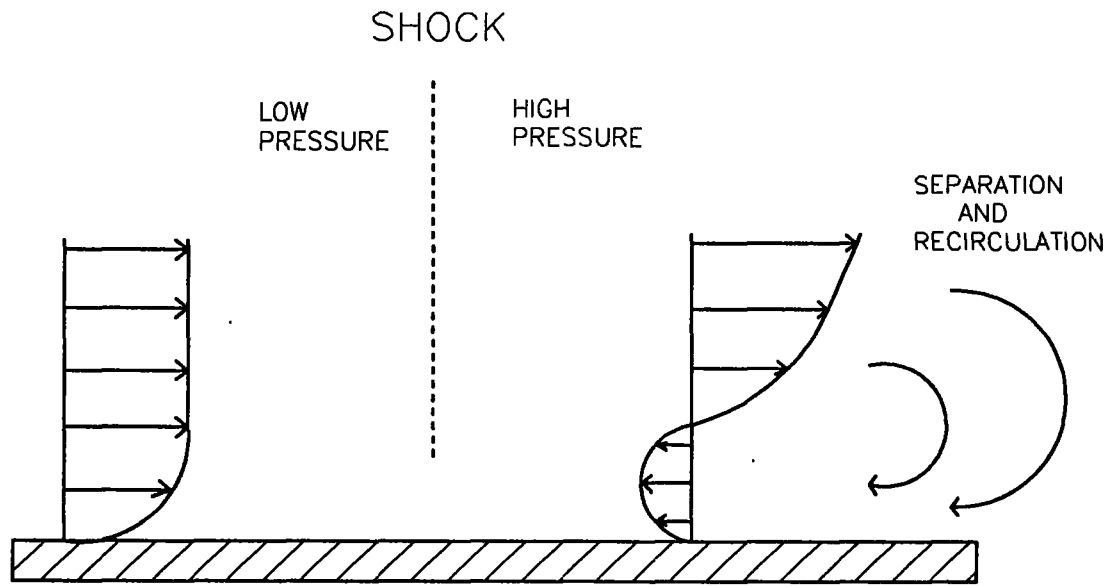

Figure 5.5. Drawing of Boundary Layer-Shock Interaction. The adverse pressure gradient across the shock causes separation.

Mach number could reduce stress on the particles preventing particle breakup.

From Fig. 5.4, the McGregor 2 probe had the least deposition of any probe tested. The McGregor 2 probe averaged 25% less deposition than the Colket 1 probe and 60% less deposition than the Dehne 1 probe. Because the McGregor 2probe had no sudden expansions or shock-boundary layer interactions, less internal deposition occurred. Figure 5.6 shows the deposition in the best three probes regardless of design class. The McGregor 1 and 2 probes along with the Colket 1 probe were the best three probe designs based on deposition.

Figure 5.7 shows the losses in each McGregor probe plotted versus Willeke's deposition parameter, Ω $(St/Re^{.5})$. [19] Because Willeke's parameter is applicable to subsonic boundary layers, the parameter was used to correlate the deposition data for the McGregor probes which contained only subsonic boundary layers. In Fig. 5.7 the data for each of McGregor probe was fitted to linear least squares line. The results of the curve fit appear below:

		Correlation Coefficient
McGregor 1:	$E = 1183\ \Omega + 19.7$	.96
McGregor 2:	$E = 1011\ \Omega + 1.55$	.97
McGregor 3:	$E = 1273\ \Omega + 3.33$	.99

Shown in Fig. 5.8 are the ranges of Ω that occur under the conditions of the rocket and jet engine tests. The experimental data seemed to fall in the middle of the rocket range and slightly above the jet range. From Fig. 5.8, the correlations would always predict less deposition in the jet engine case as compared to the rocket case if the same probe was used. By calculating Ω for a particular situation and using the correlations given above, the magnitude of the

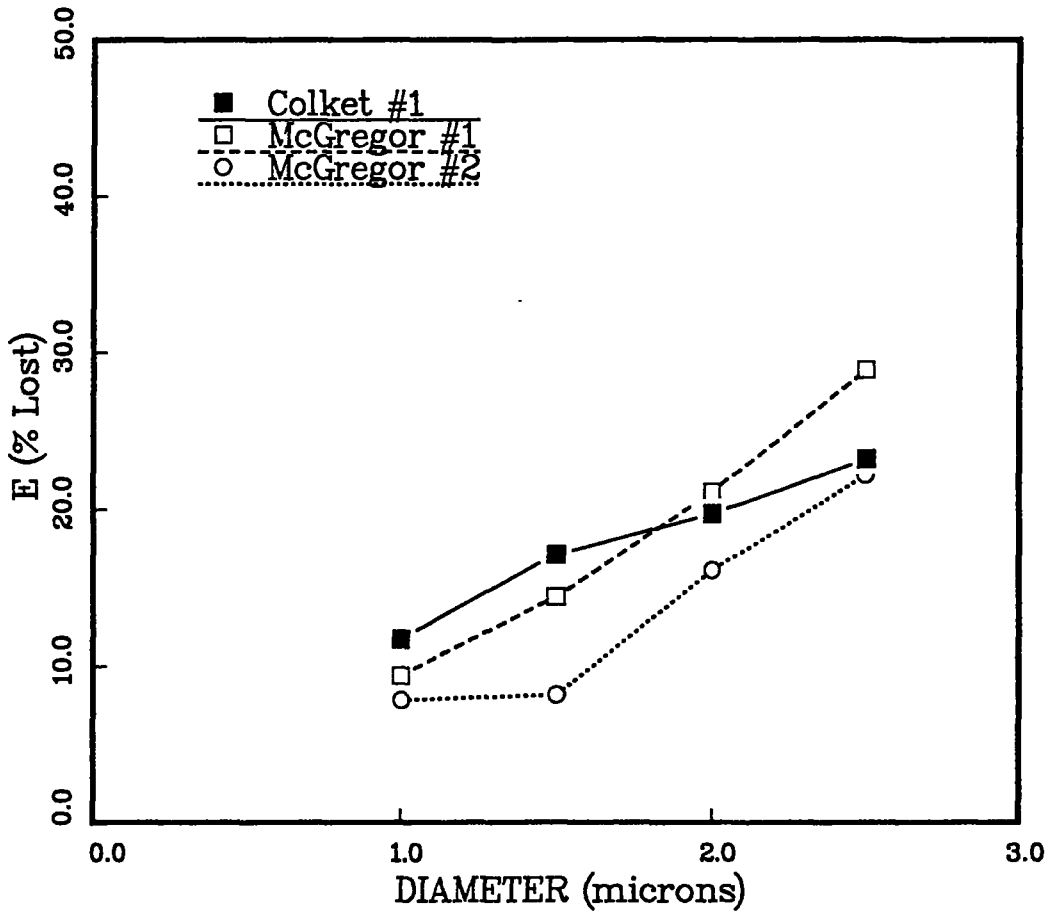

Figure 5.6. Percent of Deposited Particles (E) in the Best Three Probes versus the Particle Diameter (d_p).

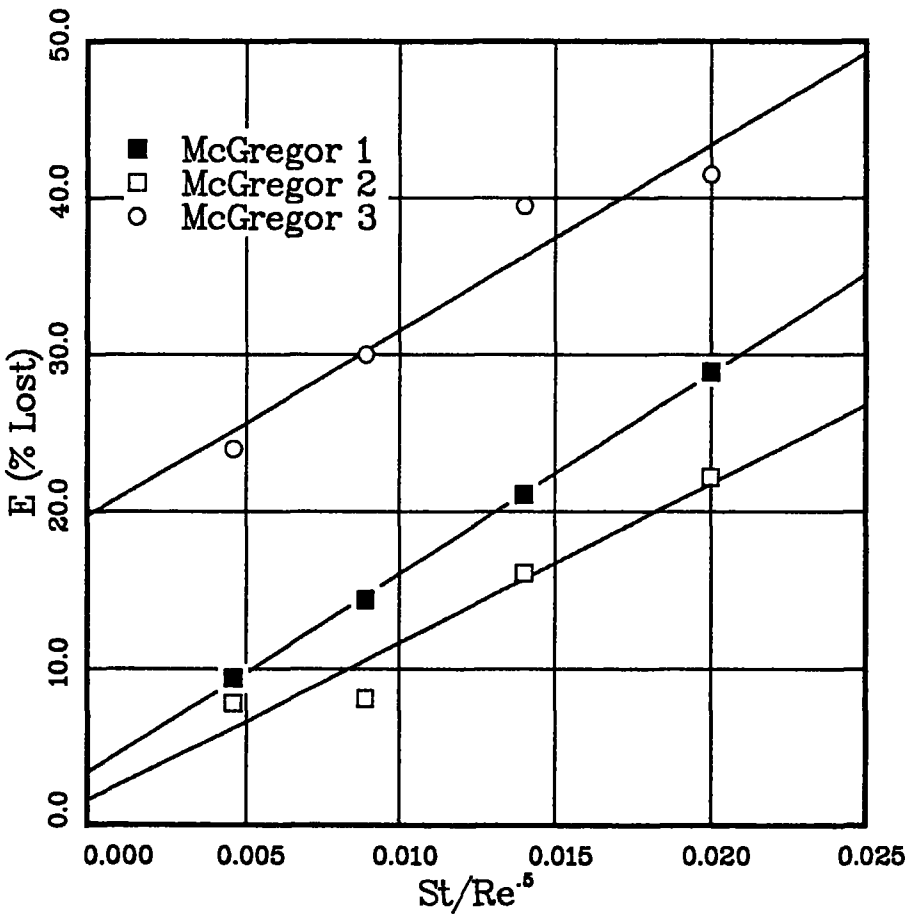

Figure 5.7. Percent of Deposited Particles (E) versus the Dimensionless Group: $St/Re^{.5}$. (Linear)

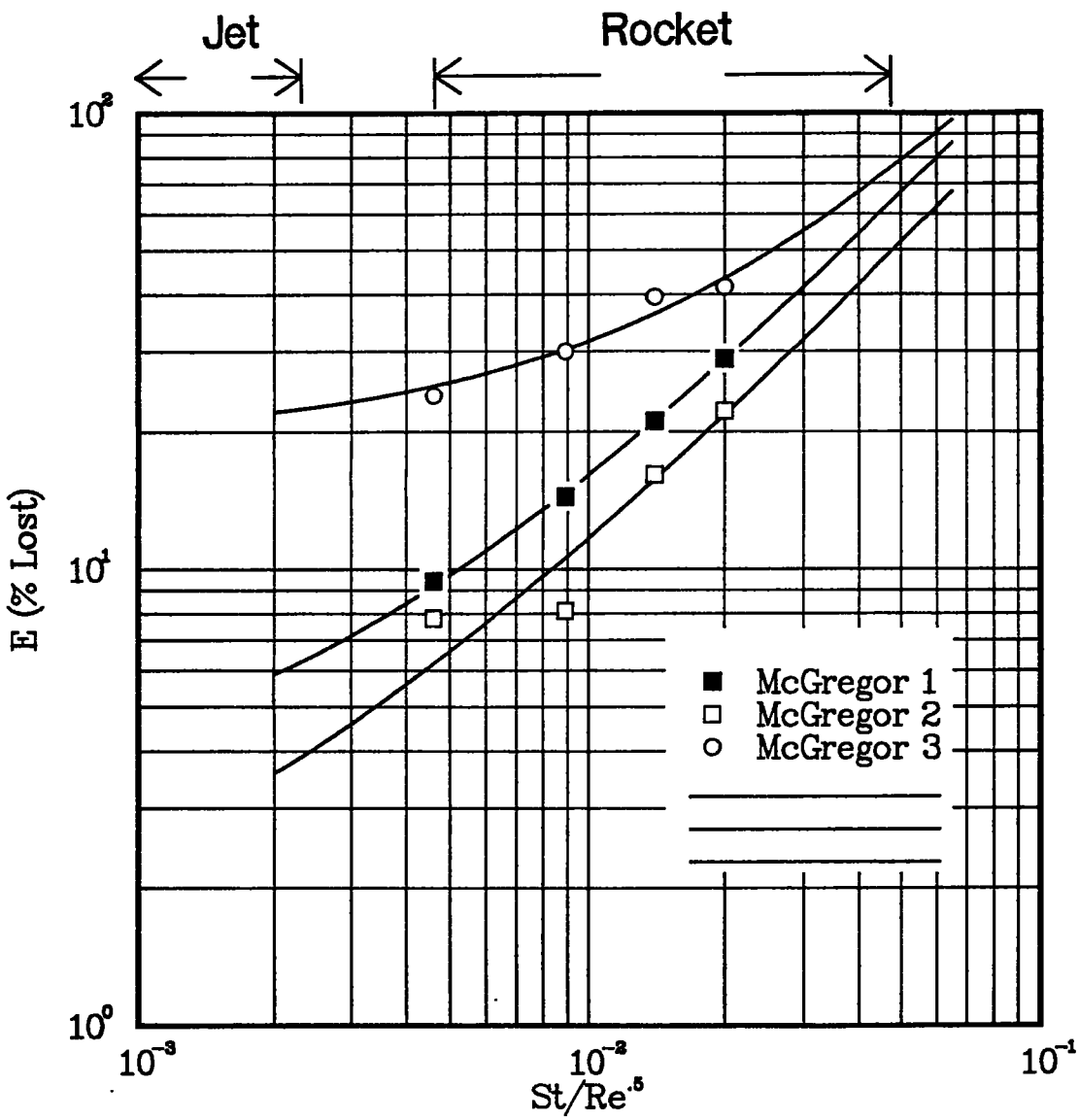

Figure 5.8 Percent of Deposited Particles (E) versus the Dimensionless Group: St/Re$^{.5}$. (Logarithmic)

internal wall losses, E, can be estimated when a McGregor probe is used.

5.2 PRESSURE RECOVERY

Another characteristic of the probes was the stagnation pressure loss across the probe. If large pressure losses are a characteristic of the probe, more attention would be needed in designing filters, valves, and pumps downstream of the probe in actual test conditions. Table 5.1 shows the stagnation pressure ratios across each of the probes. The results showed that the Dehne probes had a 60% greater pressure loss than the McGregor 1 or 2 probes. These pressure losses were attributed to the large frictional losses caused by the supersonic flow inside the probe [16]. Also the abrupt internal changes (30° diffuser and sudden expansion) between the probe and the sample line caused part of the pressure losses in the Dehne probes.

A characteristic of the Colket probes was their large stagnation pressure losses. From Table 5.1, Colket 1 had the largest pressure losses of any probe tested. The pressure losses were caused by the supersonic flow in the throat section of the probe. To position the shock at the sudden expansion, the large frictional losses in the throat were overcome by reducing the back pressure [16]. Though controlling the Colket 1 probe was straightforward, the need to maintain a low back pressure reduced the amount of instrumentation that was used on the stream ingested by the probe. In the present study, both the flowmeter and 1/2 in. gate valve of the monitoring section (Fig. 4.3) were removed to achieve the necessary back pressure. In actual test conditions, close attention would be needed in designing the equipment used to analyze the effluent stream from the probe.

TABLE 5.1

Losses in Stagnation Pressure for Each Probe Design

	P_{o2}/P_{o1}
Dehne 1	0.20
Dehne 2	0.19
Colket 1	0.07
Colket 2	0.18
McGregor 1	0.48
McGregor 2	0.48
McGregor 3	0.19

From Table 5.1, the McGregor 1 and 2 probes were the best probes based on pressure loss. Because of the smooth internal lines and small frictional losses due to subsonic flow, the probe's only significant source of stagnation pressure loss was the bow shock positioned at the mouth of the probe [6,16].The McGregor 3 probe had larger pressure losses because of the sudden expansion located between the constant area duct and the sample line. Also some losses were attributed to the near sonic flow caused by the frictional choking that occurred in the constant area duct of the probe.

5.3 EASE OF OPERATION AND CONSTRUCTION

An advantage of both the Colket and Dehne probes was their ease of operation. Because the oblique shock at the end of the supersonic expansion section tripped the boundary layer, the control of the back pressure was not critical in the Dehne probes. The oblique shock started and stabilized the shock train in the constant area section of the probe. Similarly, the sudden expansion in the Colket probes stabilized the shock train in the sample line. If the back pressure was low enough, close control was not necessary.

A disadvantage of the McGregor probes was the need to closely control the back pressure. The control of the pressure was needed so that the bow shock created by the probe could be positioned. During the operation of the McGregor probes the shock was positioned close enough to the probe entrance so that few particles spilled around the edges of the probe, but far enough away to prevent any shock-boundary layer interaction within the probe. Though in the present study several minutes were used in adjusting the back pressure, the time necessary to adjust the back pressure may not be available in actual test conditions.

A disadvantage of the Colket 1 probe was the need for aerodynamic smooth internal surfaces. Any sudden bend or surface imperfection tripped the boundary layer and caused the shock train to occur in the throat section similar to Dehne 1 and 2. Though operating the Colket 1 probe was not difficult in the present study, preserving the smooth internal surface could be a problem in actual test conditions.

All the probes were easily constructed requiring only one man-day to complete a probe. In the process, a piece of drill rod was machined to match the internal geometry of the proposed probe. After the drill rod was hardened, the rod was used to bore a hole in a metal dowel. Then the external surface of the metal dowel was machined to the proper dimensions yielding the finished probe. Several of the probes were constructed in two pieces with joint made at the sudden expansion where any imperfections could be disregarded.

5.4 PARTICLE BREAKUP

In all the probes studied, the swallowed particles were subjected to large shear forces caused by the velocity gradients across shocks. The magnitude of these shear forces was quantified by using the dimensionless group called the Weber number [30]:

$$We = \frac{\rho_2 (v_1 - v_2)^2 d_p}{\sigma} \qquad (5.1)$$

From previous studies [30,31,32] Weber numbers in the range of 10 to 20 and higher have indicated that particle breakup was likely.

From experimental evidence gathered, particle breakup did not occur in any of the test probes when 1.0, 1.5, 2.0, 2.5 μm diameter particles were used. By visually inspecting

ingested particles under a microscope, very few particle fragments were found in the samples. Particle breakup did occur when larger particles were used. When 5 μm particles were utilized, a few particle fragments were found in the sample along with a majority of whole particles. When 10 μm particles were tested, only particle fragments were seen in the sample. Calculating the Weber number for the case of a particle passing through a Mach 2.5 normal shock gave the results shown in Table 5.2.

TABLE 5.2

Weber Numbers for Various Particle Diameters at Laboratory Conditions

d_p (μm)	We
1	3
5	15
10	30

As shown above, the laboratory results correlate well with other studies that indicated critical Weber numbers between 10 and 20. For the rocket conditions (see Table 3.1), the particles greater than 10 μm in diameter would exceed the upper limit of the critical Weber number range and probably breakup.

6.0 CONCLUSIONS

The following conclusions have been made from the investigation of the seven probes tested in the present study.

1. In all the probes tested, the internal wall deposition caused the collected sample to be biased toward the smaller particles. In the present study, a 2.5 μm particle was twice as likely to deposit on the probe wall as was a 1.0 μm particle.

2. On the basis of minimizing deposition, the best three probes were as follows:

	E (average)
McGregor 2	14.0%
Colket 1	18.0%
McGregor 1	18.5%

3. The reasons for less deposition in the McGregor 1 and 2 probes were the absences of shock-boundary layer interactions, boundary layer-particle interactions, and sudden expansions.

4. The reason for less deposition in the Colket 1 probe was the thin supersonic boundary found in the supersonic constant area throat.

5. The deposition in the Dehne 1 and 2 probes was 60% greater than the deposition in the McGregor 2 probe. The increased deposition in Dehne 1 and 2 resulted from all three enhancement factors being present: shock-boundary layer

interaction, particle-boundary layer interaction, and sudden expansions.

6. The deposition at a sudden expansion was decreased if the sudden expansion was replaced with a large angle diffuser. The deposition in Dehne 1 was 20% less than Dehne 2. The only difference between the two probes was the 30° diffuser that was used in Dehne 1 instead of the sudden expansion used in Dehne 2.

7. By using Willeke's deposition parameter, Ω, the following correlations were found relating the internal wall deposition, E, to Ω for the McGregor probes.

McGregor 1:	$E = 1183\ \Omega + 19.7$
McGregor 2:	$E = 1011\ \Omega + 1.55$
McGregor 3:	$E = 1273\ \Omega + 3.33$

8. The recovery of stagnation pressure was worst in the Colket 1 probe and best in the McGregor 1 and 2 probes. Only 7.0% of the original stagnation pressure was recovered in the Colket 1 probe while 48% was recovered in the McGregor 1 and 2 probes. When using the Colket probe, equipment used to analyze the probe stream would need to be carefully designed to minimize pressure losses. Some equipment with inherently high pressure losses may have to be eliminated.

9. The most difficult probes to control while they operated were the McGregor probes. The back pressure must be manipulated to within a few percent of a set value to locate the shock at the entrance but not inside the probe mouth.

10. From visual inspection of collected particle samples, particle breakup due to particle-shock interaction was not apparent unless particles with diameters greater than 5 μm were used. Consequently, the critical Weber number that indicated particle breakup was between 15 and 30 for the present study.

11. The Colket 1 probe was the most difficult to construct because of the need to smooth all corners. Any sharp corners or surface imperfections in the internal walls of the Colket 1 probe would cause oblique shocks within the probe. These shocks with their adverse pressure gradients would lead to boundary layer separation and increased deposition.

7.0 RECOMMENDATIONS

During the progression of the present investigation several areas of interest have been uncovered that require further work. In regards to wall losses within the particle probes, the individual effects of wall discontinuities, shock-boundary layer interactions, and particle-boundary layer interactions need to be investigated. If these individual effects can be isolated and more closely quantified, better probe designs may result.

Another area for future work is the development of monitoring equipment and operating procedures to use during actual tests conditions. For example, several minutes are needed to position the McGregor probes at a point of known Mach number in the current experiment. Then more time is needed to adjust the back pressure so that the shock is positioned slightly outside the probe mouth. With probe exposure times in actual engine tests being on the order of seconds instead of minutes, proper operation of the probe cannot be attained using the current equipment and procedures. Control loops that are able to monitor and adjust the back pressure much more quickly are needed before the McGregor probes can be used in actual engine tests.

Lastly, the phenomenon of particle breakup needs to be studied. Though particle breakup in the current experiment was not apparent, larger particle stresses may occur in actual test conditions (especially rocket tests). If particle breakup does occur, the probe design may be modified to help minimize or eliminate the breakup problem.

8.0 REFERENCES

1) Martone, J.H., P.S. Daley, and R.W. Boubl, "Sampling Submicrometer Particles in Rear Sonic and Supersonic Free Jets," CEEDO-TR-77-48, Tyndall Air Force Base, Florida (1977).

2) Forney, L. J., "Scaling Laws for Particle Breakup in Nozzle Generated Shocks," Final Report - Proceedings of 1982 USAF-SCEEE Summer Faculty Research Program.

3) McGregor, W.K., P.T. Girata, and R. Quinn, "Inertial Upper Stage (IUS) Solid Rocket Motor (SRM) Core Flow Sampling at High Altitudes," AEDC-TR-83-1, Arnold Air Force Station, Tennessee (1983).

4) Dehne, H.J., "An Automatic Isokinetic Sampler for Particle Emissions from Aircraft Gas Turbine Engines," Report ESL-TR-80-4, Acurex Corp., California (1980).

5) Martone, J.A. and P.S. Daley, "Sampling Submicrometer Particles Suspended in Near Sonic and Supersonic Free Jets," Journal of the Air Pollution Control Association 30, 898(1980).

6) Forney, L.J., W.K. McGregor, and D.B. Van Dyke, "Computation of Gas Flowfield in Supersonic Particle Probes," Journal of Fluids Engineering 108, 76(1986).

7) Colket, M.B., L. Chiappetta, R.N. Guile, M.F. Zabielski, and D.J. Seery, "Internal Aerodynamics of Gas Sampling Probes," Combustion and Flame 44, 3(1982).

8) McGregor, W.K., Sverdrup Technology Inc., Arnold Air Force Station, Tennessee, private communication to L.J. Forney (1982).

9) Forney, L.J., "Aerosols in Turbulent Tube Flow: Deposition and Rebound," Ph.D. Thesis, Harvard University, Cambridge, Massachusetts (1974).

10) Forney, L.J. and Spielman, L.A., "Deposition of Coarce Aerosols from Turbulent Flow," Aerosol Science 5, 257(1974).

11) Fuchs, N.A., "Review Paper on Sampling of Aerosols," Atmospheric Environment 9, 697(1975).

12) Belyaev, S.P. and L.M. Levin, "Techniques for Collection of Representative Aerosol Samples," Aerosol Science 5, 325(1974).

13) Parker, G.J., "Some Factors Governing the Design of Probes for Sampling in Particle- and Drop-Laden Streams," Atmospheric Environment 2, 447(1968).

14) Forney, L.J., W.K. McGregor, and D.B. Van Dyke, "Dynamics of Particle-Shock Interactions: Part 1: Similitude," Aerosol Science and Technology 6, 129(1987).

15) Forney, L.J. and W.K. McGregor, "Particle Sampling in Supersonic Streams with a Thin-Walled Cylinderical Probe," AIAA Journal 25, 1100(1987).

16) Shapiro, A.H., Compressible Fluid Flow, Ronald Press, New York (1953).

17) Frielander, S.K., Smoke, Dust, and Haze, John Wiley, New York, 1976.

18) Israel, R. and D.E. Rosner, "Use of a Generalized Stokes Number to Determine the Aerodynamic Capture Efficiency of Non-Stokesian Particles from a Compressible Gas Flow," Aerosol Science and Technology 2, 45(1983).

19) Willeke, K. and K. Okazaki, "Transmission and Deposition Behavior of Aerosols in Sampling Inlets," Aerosol Science and Technology 7, 275(1987).

20) Reeks, M.W. and G. Skyrme, "The Dependence of Particle Deposition Velocity on Particle Inertia in Turbulent Pipe Flow," Journal of Aerosol Science 7, 485(1976).

21) Wildi, J. and H. Thomann, "Measurement of Deposition of Small Particles in Stationary and Oscillating Turbulent Pipe Flow," Journal of Aerosol Science 14, 615(1983).

22) Schlichting, H. Boundary Layer Theory, McGraw-Hill, New York, 1979.

23) Crocco, L., "Sullo Strato Limite Laminare Nei Gas Lungo Una Lamina Prana," Rend. Mat. Univ. Roma. 7, 138(1941).

24) Gilstrap, W.A. and J.J. Carlson, "Performance and Recovery in Conical, Straight-Walled Diffusers," Engineering Report 48, University of Nevada, Reno, Nevada (1974).

25) Patterson, G.N., "Modern Diffuser Design," Aircraft Engineering 10, 267(1938).

26) Liu, B.Y.H. and D.Y.H. Liu, "Generation of Monodisperse Aerosol Standards," Environmental Science and Technology 7, 147(1973).

27) Cooper, D.W. and P.C. Reist, "Neutalizing Charged Aerosols with Radioactive Source," Journal of Colloid and Interface Science 45, 17(1973).

28) Berglund, R.N. and B.Y.H. Liu, "Drop Size Measurement of Liquid Aerosols," Atmospheric Environment 16, 563(1982).

29) Welty, J.R., C.E. Wilson, and R.E. Wilson, Fundamentals of Momentum, Heat, and Mass Transfer, John Wiley, New York, 1976.

30) Clift, R., J.D. Grace, and M.E. Weber, Bubbles, Drops, and Particles, Academic Press, New York, 1978.

31) Bartlett, R.W., and L.J. Delaney, "Effect of Liquid Surface Tension on Maximum Size in Two Phase Flow," Pyrodynamics 4, 337(1966).

32) Caveny, L.H. and A. Gany, "Breakup of Al/Al_2O_3 Agglomerates in Accelerating Flowfields," AIAA Journal 17, 1368(1979).

33) van Driest, E.R., "Turbulent Boundary Layers in Compressible Fluids," Journal of Aeronautical Science 18, 145(1951).

34) Ackeret, J., Aspects of Internal Flow, Elsevier Publishing Co., New York, 1967.

35) Hinds, W.C., Aerosol Technology, John Wiley, New York, 1982.

36) Crowe, C.T., "Drag Coefficient of Particles in a Rocket Nozzle," AIAA Journal 5, 1021(1967).

APPENDIX A. NOMENCLATURE

A = probe cross sectional area (m^2)

A1 = compressibility correction factor

c = speed of sound (m/s)

C = drag coefficient for a sphere

C_f = skin friction coefficient

d = probe entrance diameter (m)

D = sample line diameter (m)

D_d = diffusion coefficient

d_p = particle diameter (m)

E = particle deposition losses in probe (%)

f = fanning friction factor

Kn = Knudsen number

L = length of probe (m)

L_s = length of sample line (m)

L_T = length of probe including sample line (m)

M = Mach number

P = pressure (kg/m s^2)

R = gas constant (m^2/s^2 K)

Re = probe Reynolds number

Rep = particle Reynolds number

Re_x = Reynolds number based on duct length

St = particle Stokes number

T = temperature (K)

t = time (s)

v = velocity (m/s)

v_{ave} = average velocity (m/s)

v_d = deposition velocity (m/s)

v_r = relative velocity (m/s)

We = Weber number

x = distance from probe entrance (m)

δ = boundary layer thickness (m)

δ_d = diffusional boundary layer thickness (m)

γ = ratio of specific heats

μ = gas viscosity (kg/m s)

ν = kinematic gas viscosity (m^2/s)

ρ = gas density (kg/m^3)

ρ_p = particle density (kg/m^3)

σ = surface tension of particle (kg/s^2)

ϕ_c = Cunningham slip factor

ϕ_r = non-Stokesian correction factor

ψ_s = Stokes number based on Stokesian drag

ψ = corrected Stokes number (St)

Ω = $St/Re^{.5}$

Subscripts

1 = static conditions before shock

2 = static conditions after shock

o1 = stagnation conditions before shock

o2 = stagnation conditions after shock

p = particle property

g = gas property

APPENDIX B. CORRELATION OF PRESSURE DATA

To verify the internal flow fields in the probes, the pressure data of four probes was fitted to a one-dimensional, gas-dynamic model. Because of the absence of large temperature gradients and reacting flows, the one-dimensional model took the form [16]: (fanno flow)

$$\frac{dM^2}{M^2}(1-M^2) = -2\left[1 + \frac{\gamma-1}{2}M^2\right]\frac{dA}{A} + \gamma M^2\left[1 + \frac{\gamma-1}{2}M^2\right]4f\frac{dx}{D} \qquad (B.1)$$

where the first term on the right hand side was the effect of flow area variation and the second term was the effect of skin friction on the flow. By solving Eq. B.1 the Mach numbers at various locations were calculated and then from continuity, the pressures in the probe were calculated. The friction factor, f, in Eq. B.1 was used to fit the equation to the pressure data of the present study.

Figure B.1 shows the pressure data collected from the Dehne 1 probe and the result of Eq. B.1. Recalling the internal structure of Dehne 1 (Fig. 2.2), the flow travels through a supersonic diffuser in the initial 0.8 in. of the probe. As the area of the probe expands, the Mach number increases while the static pressure decreases. At the transition between the diffuser and the constant area throat, the sharp corner causes an oblique shock that produces a pressure rise. This pressure rise trips the boundary layer and causes a shock train in the constant area throat of the probe. Instead of having the shock train extend over a length of 8 to 10 pipe diameters, the model compresses the shock train into one normal shock that occurs at approximately 1.5 in.

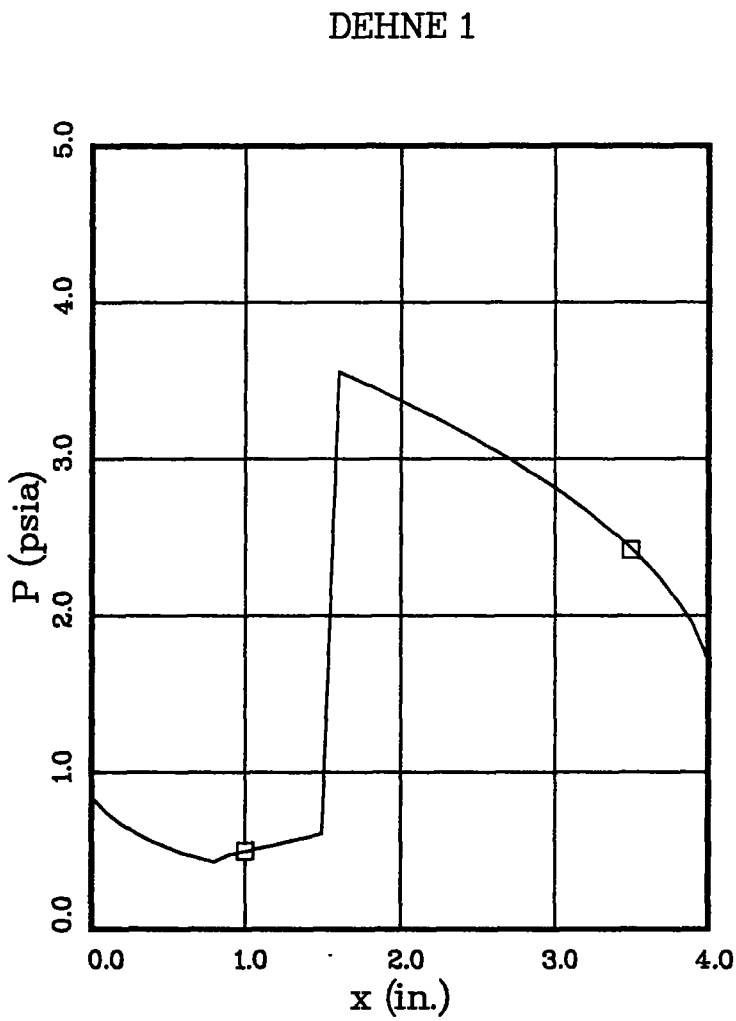

Figure B.1. Pressure Correlation in the Dehne 1 Probe.

After the shock, the frictional choking in the constant area throat causes the subsonic flow to increase in velocity and decrease in pressure until the end of the throat.

The friction factors, f, used in the model were 0.0088 in the initial supersonic section and 0.037 in the subsonic section of the probe. The value for the supersonic section is within 10% of the measured friction factor for flow in a smooth pipe with a Re=20,000 [33]. The value in the subsonic section is twice the value reported [29]. The reason for the difference may be the incorrect location of the shock train within the constant area throat.

Figure B.2 shows the pressure data collected on the Colket 1 probe and the fit of equation B.1 to that data. Recalling the internal structure of Colket 1 (Fig. 2.5), the flow travels through a supersonic diffuser in the initial 1.2 in. of the probe. Unlike Dehne 1, the transition between the expansion and the constant area throat is aerodynamically smooth so that no oblique shock occurs. In the supersonic constant area throat, the frictional choking causes a reduction in Mach number and an increase in static pressure. The friction factor used in the model was 0.0032 that is within 20% of the reported friction factors for supersonic flow in a smooth pipe [16,33].

Figure B.3 and B.4 show the pressure data collected from the McGregor 1 and 3 probes and the fit of Eq. B.1 to the data. In McGregor 1, a 3.5° subsonic diffuser extends the entire 4 in. length of the probe. The area expansion causes the velocity to drop and the pressure to rise. In the McGregor 3 probe, the constant area throat extends the entire 4.0 in. of the probe. The frictional choking causes an acceleration of the subsonic flow and a decrease in the static pressure. At the end of the throat, the choking causes near sonic flow indicated in Fig. B.4 by the leveling off of the static pressure. The friction factors were 0.059 for McGregor

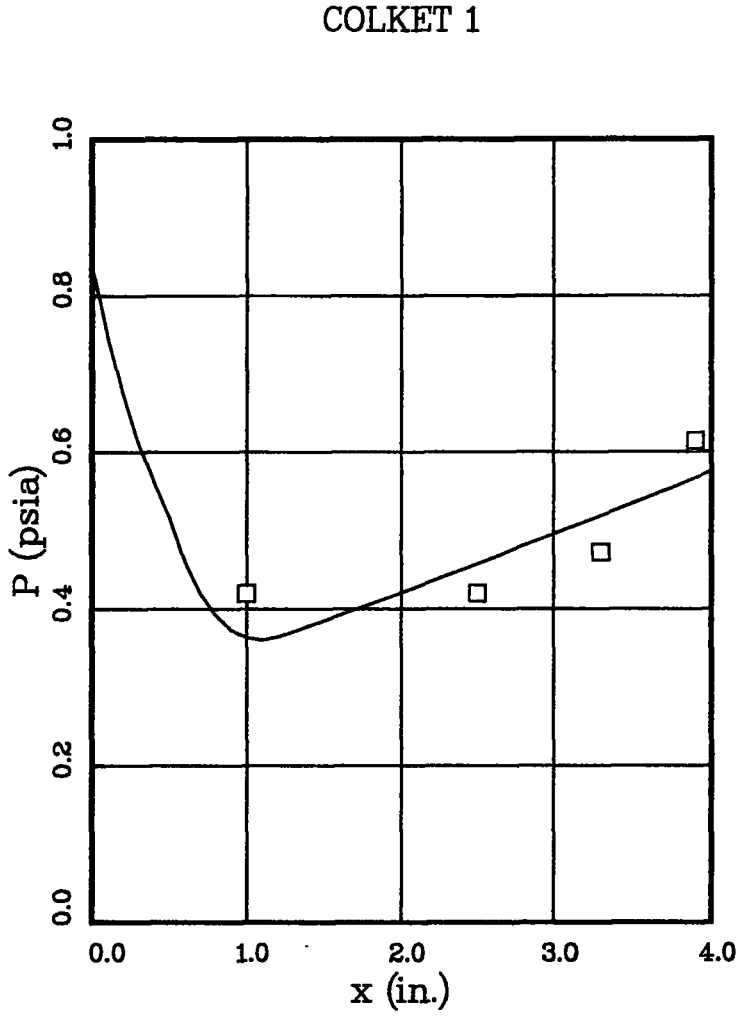

Figure B.2 Pressure Correlation in the Colket 1 Probe.

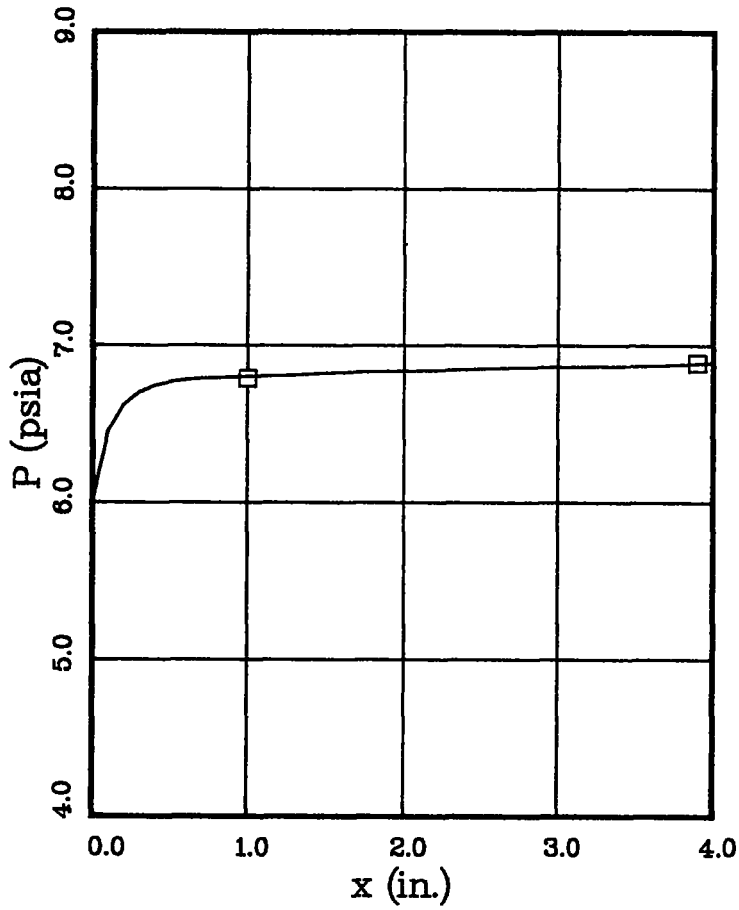

Figure B.3. Pressure Correlation in the McGregor 1 Probe.

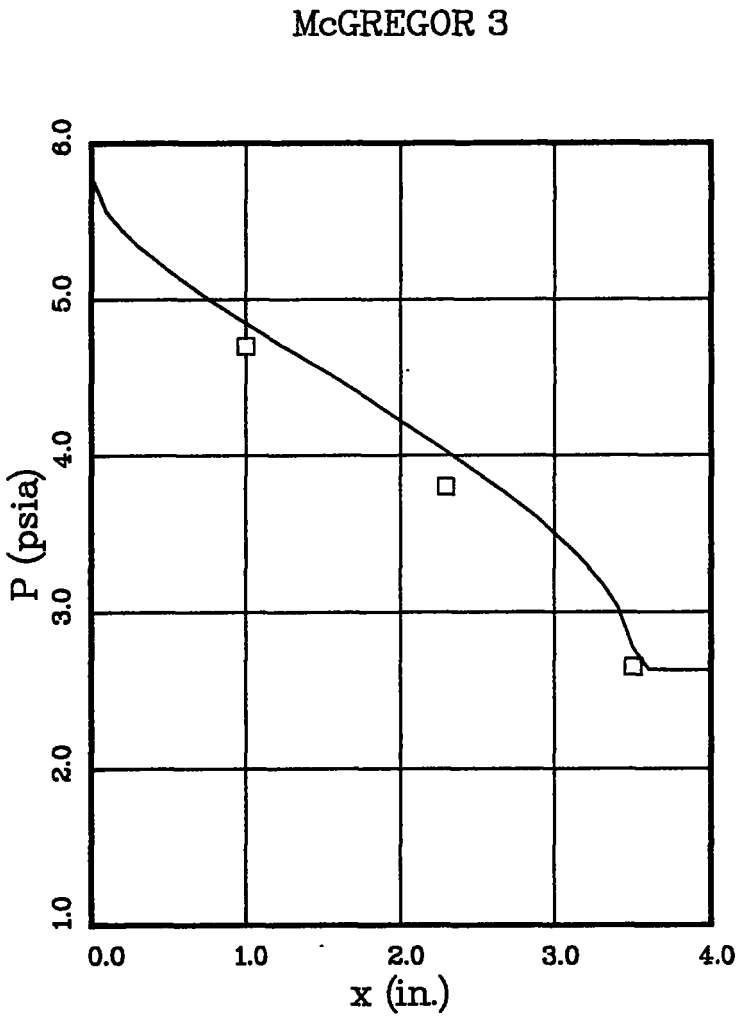

Figure B.4. Pressure Correlation in the McGregor 3 Probe.

1 and 0.013 for McGregor 3. These factors are within 10% of the reported values under similar conditions [29,34].

The computer program PRESSURE on the following page was used to solve Eq. B.1 to calculate the pressure profile in the Colket 1 probe. An IMSL (International Mathematics and Statistical Library) routine using Gear's method was used to integrate. The other computer program BLAYER is a combination of the PRESSURE program and the boundary layer thickness correlations given in Chapter III. In this program the thickness of the boundary layer in the McGregor 3 probe is calculated.

```
                PROGRAM PRESSURE

C
C               Define Variables
C
      REAL Y(1),WK(18),X,TOL,XEND,H,RHOI,TO,AF,AI,MI,TI,R,C,
     &     F,M(100),T(100),P(100),A(100),PO(100),RHO(100),L
      INTEGER N,K,METH,MITER,INDEX,IWK(1),IER
      COMMON/BL1/F,C,DS,DI,DF,L
      EXTERNAL FCN,FCNJ
C
C
C               Initialize Variables
C
      MI=2.5
      POI=14.34
      PI=POI*(1.+0.2*MI**2)**-3.5
      TO=537.
      PIE=3.1416
      AF=.0276
      AI=.0192
      TI=TO/(1.+.2*MI**2)
      R=639.4
      RHOI=PI/(R*TI)
      PRINT*,'INPUT F'
      READ*,F
      L=0.5
      C=L*AI/(AF-AI)
      DI=5./32.
      DF=6./32.
      DS=(DF-DI)/L
      N=1
      X=0.0
      XD=1.0
      PD=.42
      Y(1)=MI**2
      TOL=.00001
      H=.00001
      METH=1
      MITER=1
      INDEX=1
      PRINT*,'L=',L,'  F=',F
      PRINT*
      PRINT*,'    X           STATIC P        STAGN P
     &       MACH #'
      PRINT*,X,PI,POI,MI
C
```

```
C
C
C                Calculate Mach #, Temperature, Density,
C                and Pressure in Probe
C
C
         DO 10 K=1,40
C
C                Counter used to Step off Length of Probe
C
            XEND=0.1*FLOAT(K)
C
C                Call IMSL Routine: DGEAR
C                to integrate Equation identified
C                in subroutine FCN.
C
C
            CALL DGEAR(N,FCN,FCNJ,X,H,Y,XEND,TOL,METH,
     &                  MITER,INDEX,IWK,WK,IER)
            IF (IER .GT. 128) GOTO 100
C
C                Calculation of Mach # and Temperature
C
            M(K)=Y(1)**.5
            T(K)=TO/(1+.2*M(K)**2)

C
C                Calculation of Area Variation in Probe
C
            IF (XEND .LE. L) THEN
               A(K)=(AF-AI)*XEND/L+AI
             ELSE IF (XEND .LE. 1.2) THEN
                  A(K)=PIE*((60.27+2.4*XEND-XEND**2)**.5-
     &                 7.6368)**2./4
             ELSE
                  A(K)=PIE*((60.27+2.4*1.2-1.2**2)**.5-
     &                 7.6368)**2./4
            ENDIF
c
c                Calculation of Density and Pressure
c
         RHO(K)=RHOI*AI*MI*(TI/T(K))**.5/(A(K)*M(K))
         P(K)=RHO(K)*R*T(K)
         PO(K)=P(K)*(1+.2*M(K)**2)**3.5
C
C                Print Out of Results
C
         PRINT*,XEND,P(K),PO(K),M(K),xd,pd
 10      CONTINUE
C
```

```
C
C                Check Predicted Pressure Against
C                Measured Pressure and Calculate
C                Error. Guess New Friction Factor
C                Until Error is Minimized.
C
C
      ERROR=(P(10)-.42)**2+(P(25)-.42)**2+(P(33)-.47)**2+
     &      (P(39)-.614)**2
 25   PRINT*,'ERROR = ',ERROR
 100  STOP
      END
C
C                Subroutine Defines Equation for DGEAR to
C                Integrate
C
      SUBROUTINE FCN(N,X,Y,YPRIME)
         REAL Y(N),YPRIME(N),X,F,C,DS,DI,DF,L
         INTEGER N
         COMMON/BL1/F,C,DS,DI,DF,L
C
C                Derivative Definitions for Mach #
C                At the Various Diameters in the Probe
C
C
         IF (X .LE. L) THEN
            YPRIME(1)=Y(1)*(1.+.2*Y(1))/(1.-Y(1))*(-2/(X+C)+
     &                 5.6*Y(1)*F/(DS*X+DI))
         ELSE IF (X .LE. 1.2) THEN
            D1=(60.27+2.4*X-X**2)**.5-7.6368
            DD=.5*(60.27+2.4*X-X**2)**(-.5)*(2.4-2*X)
            YPRIME(1)=Y(1)*(1.+.2*Y(1))/(1.-Y(1))*(-4*DD/D1+
     &                 5.6*Y(1)*F/D1)
         ELSE
            D1=(60.27+2.4*1.2-1.2**2)**.5-7.6368
            YPRIME(1)=Y(1)*(1.+.2*Y(1))/(1.-Y(1))*5.6*Y(1)*F/D1
         ENDIF
         RETURN
         END
C
C                          Dumby Subroutine
C
      SUBROUTINE FCNJ(N,X,Y,PD)
         INTEGER N
         REAL Y(N),PD(N,N),X
         RETURN
         END
```

```
      PROGRAM BLAYER
c
c
c          Program Description: This program calculates the
c         boundary layer thickness in the McGregor 3 probe.
c         First, a differential equation is solved to calculate
c         the Mach number along the length of the probe taking
c         into account both area variations and friction.  Then
c         by using this Mach number, the boundary layer thickness
c         is calculated.
C
C                 Define Variables and Arrays
C
      REAL Y(1),WK(11),X,TOL,XEND,H,RHOI,TO,AF,AI,MI,TI,R,C,
     &     KVISO,KVIS,F,M(100),T(100),P(100),A(100),PO(100),
     &     RHO(100),L
      INTEGER N,K,METH,MITER,INDEX,IWK(1),IER
      COMMON/BL1/F,C,DS,DI,DF,L
      EXTERNAL FCN,FCNJ
C
C                 Initialize Variables
C
      PIE=3.1416
      KVISO=2.3E-4
      MI=.487
      POI=6.8
      PI=POI*(1.+0.2*MI**2)**-3.5
      TO=537.
      TI=TO/(1.+.2*MI**2)
      R=639.4
      RHOI=PI/(R*TI)
      PRINT*,'INPUT F'
      READ*,F
      DI=5./32.
      N=1
      X=0.001
      Y(1)=MI
      TOL=.01
      H=.000001
      METH=2
      MITER=0
      INDEX=1
c
c               Calculate Mach #, Temperature, Density, Pressure
C               and Boundary Layer Thickness
c
      DO 10 K=1,40
```

```
c
c                Counter used to Step off Length of Probe
c
              XEND=0.1*FLOAT(K)
c
c                Call IMSL Routine:  DGEAR
c                to integrate equation identified
c                in subroutine FCN.
c
              CALL DGEAR(N,FCN,FCNJ,X,H,Y,XEND,TOL,METH,MITER,INDEX,
     &                   IWK,WK,IER)
              IF (IER .GT. 128) GOTO 100
c
c                Calculation of Mach #, Pressure, Temperature
c                Density
c
              M(K)=Y(1)
              T(K)=TO/(1+.2*M(K)**2)
            RHO(K)=RHOI*MI*(TI/T(K))**.5/(M(K))
            P(K)=RHO(K)*R*T(K)
            PO(K)=P(K)*(1+.2*M(K)**2)**3.5
c
c                Calculation of Viscosity, Velocity, Reynolds
c                Number, and Boundary Layer Thickness
c
            KVIS=KVISO*(PO(K)/P(K))*(T(K)/TO)**1.75
            VEL=M(K)*49.1*T(K)**.5
            REL=(XEND/12)*VEL/KVIS
            DLL=4.8*EXP(.236*M(K))/REL**.5
               IF (M(K) .GT. 1.2) THEN
            CFCI=-.156*M(K)+1.087
               ELSE
            CFCI=-.0833*M(K)+1
               ENDIF
            CFI=0.0576/REL**.2
            DLT2=4.1E-6/((CFI*CFCI)**4*REL)
            DLT=.37/REL**.2
            DL=XEND*DLL
            DT=XEND*DLT
            DT2=XEND*DLT2
            IF (REL .LT. 5.E5) THEN
               BL=DL
             ELSE
               BL=DT2
            ENDIF
c
c                Rescale Boundary Layer Thickness to
c                Probe Dimensions
c
            WALL1=.0775
```

```
      WALL2=-WALL1
      PROJ1=.0775
      PROJ2=-.0775
      DLG1=WALL1-BL
      DLG2=WALL2+BL
      DTG1=WALL1-DT2
      DTG2=WALL2+DT2
      PRINT*,XEND,WALL1,WALL2,PROJ1,PROJ2,DLG1,DLG2
 10   CONTINUE
 100  STOP
      END
C
C          Subroutine used to Define Equation that
c          Relates Mach number to Area Variation
c          and Friction Losses
C
      SUBROUTINE FCN(N,X,Y,YPRIME)
         REAL Y(N),YPRIME(N),X,F,C,DS,DI,DF,L
         INTEGER N
         COMMON/BL1/F,C,DS,DI,DF,L
            f1=f/(1.3e5*x)**.5
            YPRIME(1)=2.8*F1*Y(1)**3*(1.+.2*Y(1)**2)/
     &                 (DI*(1.-Y(1)**2))
         RETURN
         END
C
C           Dumby Subroutine
C
      SUBROUTINE FCNJ(N,X,Y,PD)
         INTEGER N
         REAL Y(N),PD(N,N),X
         RETURN
         END
```

APPENDIX C. PARTICLE LAG

In the experiment, the drops were accelerated from rest to a velocity of Mach 2.5 within a fraction of a second. Because of inertial effects, the drops would tend to lag behind the rapidly accelerating gas stream. If lagging occurred the drops may not be traveling at the desired velocity of Mach 2.5 at the entrance of the probe. In fact, the particles may be traveling at speeds significantly less than Mach 2.5.

To determine if the particle lag causes the above mentioned problem, a calculation was performed. From the force balance, the following expression was obtained for the relative particle acceleration [35]:

$$\frac{d(v_r)}{dt} = \frac{0.75\ C\ \rho_g\ v_r^2}{\rho_p\ d_p} \qquad (C.1)$$

where
- C = drag coefficient
- ρ_g = gas density (g/cm)
- v_r = relative particle velocity (v_g-v_p) (cm/s)
- ρ_p = particle density (g/cm)
- d_p = particle diameter (cm)
- t = time (s)

In the motion equation of the drop, the drag coefficient developed by Crowe [36] was used because his coefficient was applicable to compressible, high velocity flows. Crowe's drag coefficient takes the form [36]:

$$C = (C_{inc}-2)\exp(-3.07\gamma^{.5}(M/Re)g) + \left(\frac{h}{\gamma^{.5}M}\right)\exp\left(\frac{-Re}{2M}\right) + 2 \qquad (C.2)$$

where C_{inc} = incompressible drag coefficient for sphere

$\log_{10}(g) = 1.25(1+\tanh(0.77\log_{10}Re-1.92))$

$h = (2.3+1.7(T_p/T_g)^{.5})-2.3\tanh(1.17\log_{10}M))$

T_p = particle temperature (K)

T_g = gas temperature (K)

v_g = gas velocity (cm/s)

v_p = particle velocity (cm/s).

With the motion equation and Crowe's drag coefficient, the percent of particle lag $[100(v_g-v_p)/v_g]$ has been calculated as a function of distance the particle travels horizontally through the nozzle. Basing the calculation on a $v_p = 0$ at the throat of the supersonic converging-diverging nozzle and a gas velocity of M = 1 at the same point, the percent lag of the drop has been graphed in Fig. C.1. From Fig. C.1 the particle lag is seen to decrease below 5% for all particles when the particles travel 1.0 in. past the throat of the nozzle. Since the mouth of the probe is positioned approximately 5.0 in. from the throat of the nozzle, the particles should not be lagging the gas velocity by more than 5%. Therefore, particle lag should not affect the experimental measurements.

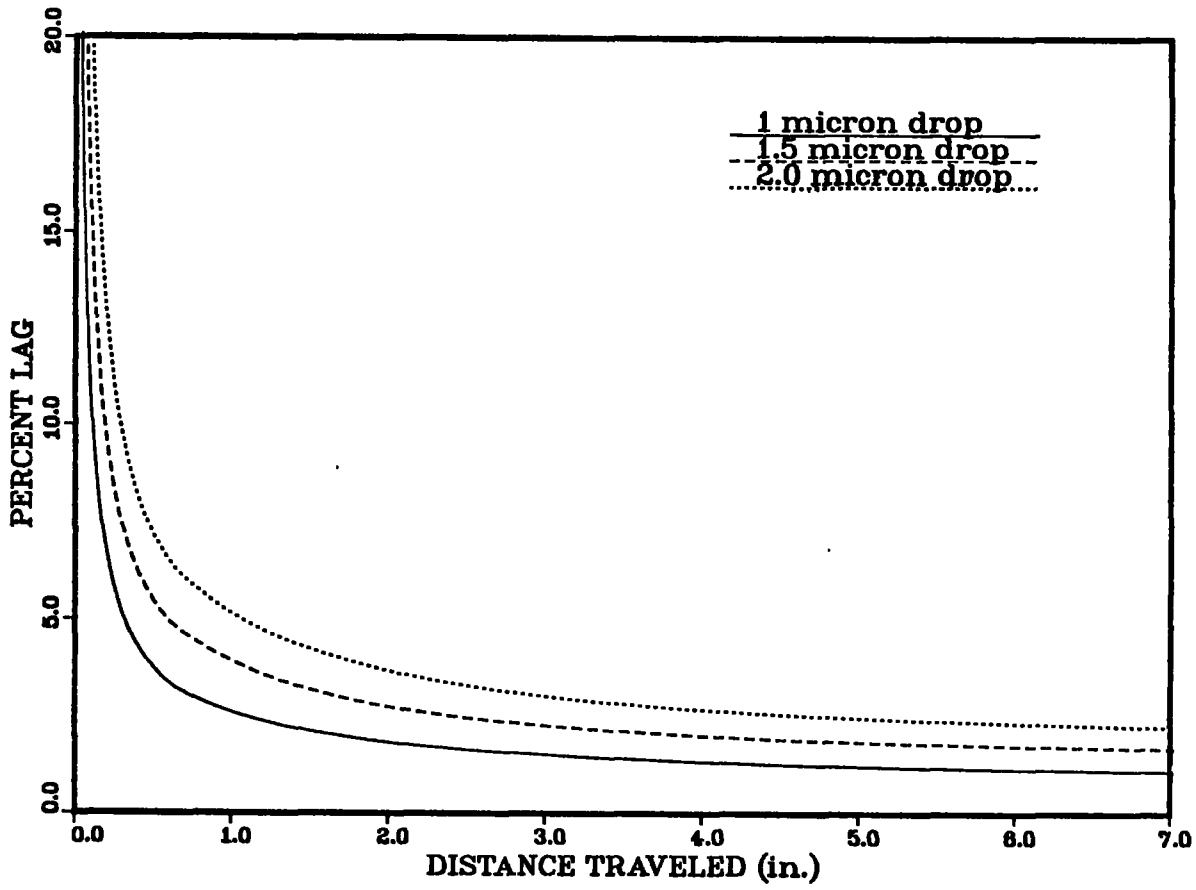

Figure C.1. Percent Lag in Drop Velocity versus the Distance the Drop Travels.

APPENDIX D. EXPERIMENTAL DATA

Tables D.1 through D.8 contain the experimental data collected on each probe. Tables D.1 through D.7 contain the fluorescence data obtained from the alcohol washes of the internal probe surfaces and the filter paper. From preliminary studies of the sample line between the probe and the filter, particle losses of 2% or less were found. Therefore, the sample line washes were discontinued. In Tables D.1 through D.7 the following information is listed:

1st column: run identification number
2nd column: diameter of particles exposed to probe (μm)
3rd column: alcohol fluorescence reading from filter wash
4th column: alcohol fluorescence reading from probe wash
5th column: sum of columns 3 and 4
6th column: percent of total fluorescence in probe wash.

Because the fluorescence reading is directly proportional to the concentration of tracer (uranine), the amount of deposition within the probe is given in column six.

Table D.8 shows the pressures and mass flow rate measured while each of the probes was operating. The pressures in the Dehne probes and the Colket 1 probe were closely monitored to insure the shock was positioned correctly. In the Dehne probes, the pressure at P_1 rapidly decreased as the shock passed the tap. The pressure in P_3 also increased but at a slower rate. As the vacuum tank pressure increased, P_3 would slowly increase signifying subsonic flow at P_3 while P_1 remained unchanged during the test. In the Colket 1 probe, the pressures at P_1, P_2, and P_3 would increase rapidly and remain

unchanged throughout the experiment.

The mass flow rates shown in Table D.8 were the choked flow rates in the case of Dehne 1,2 and Colket 1,2 probes. The flow rates in the McGregor probes were adjusted to 95% of the choked flow rate to maintain the shock outside the probe. The mass flow rate was not measured for the Colket 1 probe because the mass flow meter had too great a pressure drop to allow the shock to travel to the sudden expansion of the probe. Therefore, the flow meter was removed from the system and replaced with a piece of 3/4 in. tubing.

TABLE D.1

DEHNE 1 PROBE

RUN #	DIAM.	FILTER	PROBE	TOTAL	PERCENT LOSS
5.00	2.00	23.50	6.90	30.40	22.70%
8.00	2.00	21.50	7.20	28.70	25.09%
9.00	2.00	72.30	19.20	91.50	20.98%
18.00	2.00	31.75	7.45	39.20	19.01%
19.00	2.00	16.75	7.35	24.10	30.50%
22.00	1.00	15.70	2.70	18.40	14.67%
26.00	1.00	7.90	4.00	11.90	33.61%
39.00	2.50	22.50	9.50	32.00	29.69%
41.00	2.50	18.70	6.68	25.38	26.32%
42.00	2.50	17.20	6.90	24.10	28.63%
43.00	2.50	15.45	6.25	21.70	28.80%
68.00	1.50	63.30	4.10	67.40	6.08%
69.00	1.50	9.00	2.44	11.44	21.33%
70.00	1.50	7.70	2.49	10.19	24.44%
127.00	1.00	6.70	1.32	8.02	16.46%

TABLE D.2

DEHNE 2 PROBE

RUN #	DIAM.	FILTER	PROBE	TOTAL	PERCENT LOSS
1	2.00	29.50	9.80	39.30	24.9%
3	2.00	19.00	10.00	29.00	34.5%
14	2.00	17.50	7.20	24.70	29.1%
15	2.00	15.30	5.60	20.90	26.8%
16	2.00	12.70	4.30	17.00	25.3%
17	2.00	20.80	6.50	27.30	23.8%
64	2.50	27.00	14.60	41.60	35.1%
65	2.50	20.60	10.30	30.90	33.3%
66	1.00	9.70	3.32	13.02	25.5%
67	1.00	9.70	3.28	12.98	25.3%
71	1.50	9.40	3.30	12.70	26.0%
72	1.50	6.40	3.30	9.70	34.0%
77	1.50	14.80	4.00	18.80	21.3%
136	1.50	4.80	1.32	6.12	21.6%
143	2.00	7.70	3.20	10.90	29.4%
146	1.00	9.72	3.09	12.81	24.1%
147	1.00	10.73	3.17	13.90	22.8%

TABLE D.3

COLKET 1 PROBE

RUN #	DIAM.	FILTER	PROBE	TOTAL	PERCENT LOSS
90.00	1.50	15.60	3.23	18.83	17.15%
91.00	1.50	13.40	2.75	16.15	17.03%
92.00	1.00	14.30	1.67	15.97	10.46%
93.00	1.00	11.90	1.83	13.73	13.33%
94.00	2.00	36.40	7.50	43.90	17.08%
95.00	2.00	32.40	9.30	41.70	22.30%
96.00	2.50	16.50	3.40	19.90	17.09%
97.00	2.50	18.10	6.00	24.10	24.90%
98.00	2.50	21.10	5.80	26.90	21.56%

TABLE D.4

COLKET 2 PROBE

RUN #	DIAM.	FILTER	PROBE	TOTAL	PERCENT LOSS
124.00	1.00	6.29	0.96	7.25	13.24%
126.00	1.00	5.34	1.01	6.35	15.91%
131.00	1.50	4.68	1.44	6.12	23.53%
132.00	1.50	3.88	1.46	5.34	27.34%
139.00	2.00	13.44	4.50	17.94	25.08%
140.00	2.00	12.72	6.09	18.81	32.38%
148.00	2.50	14.70	7.34	22.04	33.30%
149.00	2.50	16.50	7.00	23.50	29.80%

TABLE D.5

MCGREGOR 1 PROBE

RUN #	DIAM.	FILTER	PROBE	TOTAL	PERCENT LOSS
4.00	2.00	18.10	5.70	23.80	23.95%
10.00	2.00	61.90	14.83	76.73	19.33%
11.00	2.00	44.90	7.44	52.34	14.21%
12.00	2.00	40.00	6.75	46.75	14.44%
13.00	2.00	35.00	6.00	41.00	14.63%
23.00	1.00	11.20	2.60	13.80	18.84%
24.00	1.00	10.30	1.55	11.85	13.08%
25.00	1.00	12.40	2.14	14.54	14.72%
27.00	1.00	11.45	4.30	15.75	27.30%
		95% Choked Flow Rate			
37.00	2.50	23.55	9.18	32.73	28.05%
38.00	2.50	30.17	13.98	44.15	31.66%
48.00	2.50	35.20	10.00	45.20	22.12%
49.00	2.50	25.90	12.90	38.80	33.25%
50.00	2.50	21.90	10.00	31.90	31.35%
57.00	1.00	27.50	2.32	29.82	7.78%
58.00	1.00	24.10	2.97	27.07	10.97%
59.00	2.00	35.00	11.10	46.10	24.08%
60.00	2.00	51.40	11.40	62.80	18.15%
83.00	1.50	12.20	1.94	14.14	13.72%
84.00	1.50	13.90	2.48	16.38	15.14%

TABLE D.6

MCGREGOR 2 PROBE

RUN #	DIAM.	FILTER	PROBE	TOTAL	PERCENT LOSS
114.00	1.00	17.06	2.96	20.02	14.79%
115.00	1.00	16.72	2.22	18.94	11.72%
116.00	1.00	20.73	1.86	22.59	8.23%
117.00	1.50	10.23	1.04	11.27	9.23%
118.00	1.50	5.93	0.45	6.38	7.05%
119.00	2.00	31.40	5.53	36.93	14.97%
120.00	2.00	33.20	6.89	40.09	17.19%
121.00	2.50	32.10	9.37	41.47	22.59%
122.00	2.50	28.40	7.93	36.33	21.83%
129.00	1.00	12.90	1.03	13.93	73.90%

TABLE D.7

MCGREGOR 3 PROBE

RUN #	DIAM.	FILTER	PROBE	TOTAL	PERCENT LOSS
28.00	2.00	8.60	20.10	28.70	70.03%
29.00	2.00	9.00	14.20	23.20	61.21%
30.00	2.00	10.70	13.00	23.70	54.85%
31.00	2.00	10.20	13.50	23.70	56.96%
32.00	1.00	5.35	1.97	7.32	26.91%
33.00	1.00	5.25	3.75	9.00	41.67%
34.00	1.00	7.10	5.93	13.03	45.51%
35.00	1.00	3.73	1.85	5.58	33.15%
36.00	1.00	5.27	3.55	8.82	40.25%
		95% Choked Flow			
44.00	2.50	10.85	8.78	19.63	44.73%
45.00	2.50	13.05	8.68	21.73	39.94%
46.00	2.00	12.60	7.50	20.10	37.31%
47.00	2.00	9.85	7.02	16.87	41.61%
53.00	2.50	23.30	15.90	39.20	40.56%
54.00	2.50	31.10	22.90	54.00	42.41%
55.00	1.00	14.10	3.93	18.03	21.80%
56.00	1.00	13.20	4.76	17.96	26.50%
61.00	2.00	33.30	21.10	54.40	38.79%
62.00	2.00	29.80	19.80	49.60	39.92%
85.00	1.50	6.00	2.84	8.84	32.13%
86.00	1.50	7.70	2.96	10.66	27.77%

TABLE D.8

PRESSURE AND MASS FLOW RATE DATA FOR PROBES

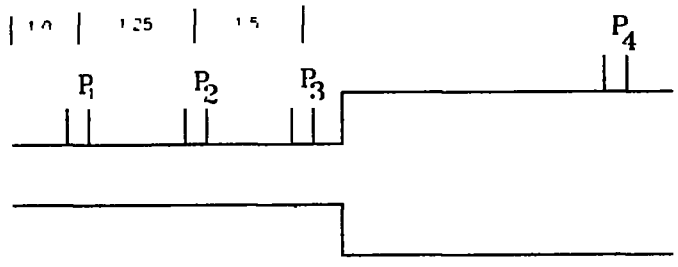

P_{o1} = atmospheric pressure

	$\frac{P_1}{P_{o1}}$	$\frac{P_2}{P_{o1}}$	$\frac{P_3}{P_{o1}}$	$\frac{P_4}{P_{o1}}$	Flow rate (g/s)
Dehne 1	0.035	--	0.17	0.20	1.15
Dehne 2	0.035	--	0.16	0.19	1.04
Colket 1	0.037	0.037	0.042	0.07	----
Colket 2	--	--	--	0.18	1.12
McGreg 1	0.45	--	--	0.48	1.06
McGreg 2	--	--	--	0.48	1.13
McGreg 3	--	--	--	0.19	1.08